Equilibrium unfolding of DLC8 monomer by urea and guanidine hydrochloride: Distinctive global and residue level features

ARTICLE *in* BIOCHIMIE · FEBRUARY 2007

Impact Factor: 2.96 · DOI: 10.1016/j.biochi.2006.09.007 · Source: PubMed

5 AUTHORS, INCLUDING:

Krishna Mohan Poluri
Indian Institute of Technology Roorkee
26 PUBLICATIONS **215** CITATIONS
SEE PROFILE

Arati Prabhu
13 PUBLICATIONS **65** CITATIONS
SEE PROFILE

Anindya Ghosh-Roy
University of California, San Diego
14 PUBLICATIONS **493** CITATIONS
SEE PROFILE

Ramakrishna V Hosur
Tata Institute of Fundamental Research
93 PUBLICATIONS **804** CITATIONS
SEE PROFILE

Available online at www.sciencedirect.com
ScienceDirect
Biochimie 89 (2007) 117–134
BIOCHIMIE
www.elsevier.com/locate/biochi

Equilibrium unfolding of DLC8 monomer by urea and guanidine hydrochloride: Distinctive global and residue level features

Amarnath Chatterjee [a], P.M. Krishna Mohan [a], Arati Prabhu [c], Anindya Ghosh-Roy [b], Ramakrishna V. Hosur [a,*]

[a] Department of Chemical Sciences, Tata Institute of Fundamental Research, Homi Bhabha Road, Mumbai 400 005, Maharashtra, India
[b] Department of Biological Sciences, Tata Institute of Fundamental Research, Homi Bhabha Road, Mumbai 400 005, Maharashtra, India
[c] Department of Pharmaceutical Chemistry, Bombay College of Pharmacy, Kalina, Mumbai 400 098, Maharashtra, India

Received 20 May 2006; accepted 5 September 2006
Available online 26 September 2006

Abstract

We present circular dichroism (CD), steady state fluorescence and multidimensional NMR investigations on the equilibrium unfolding of monomeric dynein light chain protein (DLC8) by urea and guanidine hydrochloride (GdnHCl). Quantitative analysis of the CD and fluorescence denaturation curves reveals that urea unfolding is a two-state process, whereas guanidine unfolding is more complex. NMR investigations in the native state and in the near native states created by low denaturant concentrations enabled residue level characterization of the early structural and dynamic perturbations by the two denaturants. Firstly, ^{15}N transverse relaxation rates in the native state indicate that the regions around N10, Q27, the loop between β2 and β4 strands, and K87 at the C-terminal are potential unfolding initiation sites in the protein. Amide and ^{15}N chemical shift perturbations indicate different accessibilities of the residues along the chain and help identify locations of the early perturbations by the two denaturants. Guanidine and urea are seen to interact at several sites some of which are different in the two cases. Notable among the common interaction site is that around K87 which is in close proximity to W54 on the protein structure, but the interaction modes of the two denaturants are different. The secondary chemical shifts indicate that the structural perturbation by 1 M urea is small, compared to that by guanidine which is more encompassing over the length of the chain. The probable (ϕ, ψ) changes at the individual residues have been calculated using the TALOS algorithm. It appears that the helices in the protein are significantly perturbed by guanidine. Further, comparison of the spectral density functions of the native and the two near native states in the two denaturants implicate greater loosening of the structure by guanidine as compared to that by urea, even though the structures are still in the native state ensemble. These differences in the early perturbations of the native state structure and dynamics by the two denaturants might direct the protein along different pathways, as the unfolding progresses on further increasing the denaturant concentration.

Keywords: Protein unfolding; Near native states; Secondary chemical shifts; NMR; ^{15}N relaxation; Denaturants; DLC8; Torsion angle predictions; Circular dichroism; Fluorescence

1. Introduction

For the past three decades or more, protein folding/unfolding, due to its inherent challenges, has been a frontier area of research leading to characterization of folding pathways for a number of proteins by various biophysical and computational methods [1–4]. The energy landscape view of protein folding describes the process in terms of a folding funnel, in which the broad end reflects the heterogeneous unfolded state, while the narrow end

Abbreviations: NMR, nuclear magnetic resonance; DLC8, Drosophila dynein light chain 1; GdnHCl, guanidine hydrochloride; ORF, open reading frame; CD, circular dichroism; HSQC, heteronuclear single quantum coherence; TOCSY, total correlated spectroscopy.

* Corresponding author. Tel.: +91 22 2280 4545x2488; fax: +91 22 2280 4610.
E-mail address: hosur@tifr.res.in (R.V. Hosur).

0300-9084/$ - see front matter © 2006 Elsevier Masson SAS. All rights reserved.
doi:10.1016/j.biochi.2006.09.007

reflects the supposedly homogeneous native state [5–7]. Different members of the ensemble may fold/unfold along independent pathways and their energy profiles could be different. It is believed that as the protein starts to fold it proceeds by progressive formation of native contacts and breaking of non-native contacts, if any, and eventually lands in the native conformation. Proteins that are not able to remove the non-native contacts end up getting misfolded and form aggregates becoming the cause of many diseases [8–13].

Equilibrium (un)folding studies mostly used to characterize global features of the folding–unfolding transition give definite insights into protein stabilities and structural changes that occur as the protein (un)folds. While circular dichroism and steady state fluorescence have been extensively exploited to understand the global characteristics [14–17], NMR together with hydrogen exchange and high-pressure studies has provided residue level details of the folding energy landscapes [18–22].

Urea and guanidine hydrochloride have been the two most commonly used denaturants to study the equilibrium unfolding profiles of proteins. A typical sigmoidal curve is interpreted to indicate a two-state process with a cooperative unfolding transition. That means every property measured at any denaturant concentration will be a weighted average of the properties of the folded and the unfolded states. If the cooperative unfolding is intrinsic to the protein, which may be the case for small proteins, the nature of the denaturant used would not be of much consequence. On the other hand, if the unfolding transitions measured by different probes are found to be non-identical, that is interpreted to indicate occurrence of intermediates along the transition, and the data are analyzed using three-, four- or multi-state models [15,23–25]. Theoretical simulations have supported the occurrence of intermediates along the unfolding transition [26–31]. This is more likely to be the case for larger proteins, in general, and different denaturants may have different kinds of effects. In the energy landscape view [5] this concept of fixed number of states along the unfolding transition is extended with the possibility of moving average of different partially ordered species populated at any given denaturant concentration; the partially unfolded states could arise as a consequence of multiple unfolding pathways. Cooperativity in the transitions will then be limited to small local perturbations. There have been several examples in the literature where such local unfolding transitions with limited cooperativity (sometimes termed as non-cooperative transitions) have been observed [32–39], and in one case, namely, barstar, the unfolding has been thought to be continuous incremental loss of structure [40]. Equilibrium unfolding studies in hFGF-1 presented a broad continuum of stabilities along the denaturation curve [41].

There have been several efforts in the literature to understand the mechanisms of unfolding by the two denaturants, guanidine and urea [14]. Evidence is growing to indicate that the denaturants promote unfolding by favourable interaction with groups exposed upon unfolding, rather than via generalized effects on water structure [42,43]. Guanidine and urea interact differently with the folded protein due to their unique properties [42,44–46]; guanidine is positively charged while urea is neutral. It can be envisaged, therefore, that small perturbations caused by low concentration of the various denaturants would produce different so-called near native states, and these could direct the protein along different unfolding pathways, at least in the early stages of the unfolding transition [14,44,47,48]. Thus, structural characterization of these near native states is extremely valuable to understand the unfolding initiation mechanisms in proteins. This also has a broader implication from the point of view of synergistic adaptability of protein structure, so crucial for biological function.

Dynein light chain protein (DLC8), a part of the microtubule-associated cytoplasmic dynein motor assembly is a small protein involved in a variety of intracellular motile processes such as mitosis, maintenance of Golgi apparatus, and trafficking of membranous vesicles [49]. The primary role of DLC8 appears to be as a cargo adaptor in the transport of several organelles. At physiological pH, the protein exists as a homodimer but dissociates into monomers below pH 4 [50,51]. The structure of the free monomer is identical to that of the monomer in the dimer except for small differences [52,53]. The α and β secondary structural elements in the dimer are α1: 15–31, α2: 35–50, β1: 6–11, β2: 54–59, β3: 62–67, β4: 72–78, and β5: 81–87. The corresponding secondary elements in the monomer are α1: 15–29, α2: 35–48, β1: 8–10, β2: 54–57, β4: 72–78, and β5: 81–87. Thus the differences between the two structures are (i) the β3 strand in the dimer loses its secondary structure on dissociation to the monomer and (ii) the helices α1 and α2 and the strands β1 and β2 get shortened by two residues. The dimeric form of the protein is active and binds to many cellular targets with diverse functions [54–58].

DLC8 displays pH-dependent monomer–dimer equilibrium in solution [50–52]. At pH 3.0, DLC8 is entirely monomeric. Recent folding/unfolding studies by Barbar et al. [50] using GdnHCl on the dimer at pH 6.5 showed that it unfolds via the monomeric form as the intermediate. Thus the folding and stability of the monomer are crucial to DLC8 dimer formation. In this background, we present here biophysical studies on the unfolding of the monomeric protein by the denaturants, urea and guanidine hydrochloride. We first describe the global characteristics of the unfolding phenomena, as studied by the optical techniques, and then we describe residue level detail analysis of the differences in the early unfolding perturbations caused by low concentrations of the two denaturants as studied by multidimensional NMR. These provide insights into the specific interactions between the denaturants and the protein. The data reveal that the unfolding mechanisms by the two denaturants are different. Urea unfolding is a two-state process while guanidine unfolding is more complex. The structural and dynamic characteristics of the near native states created by the two denaturants are conspicuously different.

2. Materials and methods

2.1. Construct design and protein purification

We designed a recombinant construct of DLC8 having a $(His)_6$ affinity tag at the N-terminal end of the protein. The 270 bp DLC8 ORF was amplified using a set of primers and cloned in pET-14b

vector between Nde1 and BamH1 sites. The primer set 5′-AAA AAC ACA TAT GAT GTC TGA TCG CAA-3′ and 5′-GAC GGA TCC TTA ACC GCT CTT AAA CA-3′ was used for the PCR using pUASP-DLC8 plasmid [59] as template. Positive clones were used to transform BL21-DE3 strain of *Escherichia coli*, which were grown at 37 °C in M9 minimal medium to A_{600} of ~0.6, and then induced for production of DLC8 using 0.4 mM IPTG. Uniformly ^{15}N and $^{15}N/^{13}C$ labeled protein samples were prepared by growing bacteria in M9 minimal media supplemented with 1 g l^{-1} $^{15}NH_4Cl$ and 4 g l^{-1} ^{13}C-glucose as the sole source of nitrogen and carbon, respectively, in the solution. The cells were harvested by centrifugation at 4500 rpm for 20 min using Beckman Sorvall (GSA rotor) centrifuge. The cell pellet was resuspended in extraction buffer (20 mM Tris–HCl, pH 8.0, containing 200 mM NaCl and 10 mM imidazole) containing 2.5 μg/ml leupeptin, 1 μg/ml pepstatin, 0.1 mM phenylmethylsulfonyl fluoride (PMSF), 1% Triton-X100 and 100 μg/ml lysozyme. After sonication (five shots of 15 s, constant duty cycle 60 Hz power, five times) and centrifugation (35,000 rpm, 4 °C, 45 min), the crude extract was purified by affinity chromatography on a Ni^{2+} column by eluting with 250 mM imidazole. Imidazole was removed by dialysis against extraction buffer without imidazole in a 3 kDa membrane. The $(His)_6$ tag was removed by treatment with thrombin protease for 12 h at room temperature. The protein has an extra three residue (Gly–Ser–Met) extension at its N-terminal after the cleavage of His tag. The purity of the protein sample was confirmed by SDS-PAGE.

2.2. Circular dichroism measurements

Far-UV and near-UV CD spectra were recorded at 27 °C on a JASCO model J-810 spectropolarimeter using a 1 nm bandwidth. Scans were acquired from 190 to 260 nm with a scan speed of 50 nm/min for secondary structure and from 280 to 310 nm for tertiary structure with similar scan speed. For far-UV CD, protein concentration of 20 μM was used in a fused quartz cell with a path length of 0.1 cm and for near-UV CD, protein concentration of 120 μM was used in a quartz cell of 1 cm path length. Denaturation profiles of DLC8 were measured using the aforementioned concentrations of the protein pre-equilibrated (for 12 h) with varying concentrations of the denaturants, GdnHCl and urea. At the end of these, the CD spectra for some of the denaturant concentrations were repeated. The spectra were found to be unaltered indicating that the protein had reached equilibrium before the start of the measurements. The spectra were identical irrespective of the sample preparation protocols indicating that the unfolding transition was reversible. All the measurements were repeated thrice with freshly prepared samples on different days to check for the reproducibility of the profiles. Base correction was done by recording blank experiments with different concentrations of urea and guanidine under identical conditions and subtracting this control data from that recorded with the protein. Data were first smoothened by three point averaging to minimize errors due to denaturant concentration adjustments and then normalized using the following equation [14]:

$$F_{app} = \frac{S_{obs} - S_F}{S_U - S_F} \tag{1}$$

where, F_{app} is the relative CD signal that shows the apparent unfolded fraction, S_{obs} is the observed signal at a given denaturant concentration, $S_F = k_F[D] + b_F$ and $S_U = k_U[D] + b_U$, where k_F; k_U and b_F; b_U define, respectively, the slopes and constants for the pre- and post-transition baselines and $[D]$ is the denaturant concentration.

2.3. Fluorescence measurements

Steady-state fluorescence emission spectra were recorded with $\lambda_{ex} = 295$ nm on a Spex Fluorolog-dM3000F spectrofluorimeter at 27 °C using a 1 cm path-length cuvette with a band pass of 1.5 nm for both excitation and emission. Excitation at 295 nm ensures that the emission is dominated by tryptophan fluorescence. Emission spectra were taken between 310 and 400 nm at a scan rate of 1 nm s^{-1}. Denaturation profiles of 5 μM DLC8 in acetate buffer (20 mM, pH 3.0), pre-equilibrated (for 12 h) with varying concentrations of denaturants were measured, by monitoring emission at 330 nm. Data were normalized using the following equation [14]:

$$F_{app} = \frac{S_F - S_{obs}}{S_F - S_U} \tag{2}$$

where, the individual entities have the same definition as above.

2.4. Data analysis

The data for unfolding transitions probed by CD and fluorescence were quantitatively analyzed according to two-state (N ⇔ U) and three-state (N ⇔ I ⇔ U) transition models. The equations for these models were obtained from the equation for fitting multi-state transition derived from the law of mass action concept described previously [60,61]. Thus we have Eqs. (3) and (4) for fitting the data to two-state and three-state transitions, respectively.

$$A_{obs} = \frac{A_0 + A_{11}\exp - \dfrac{\left(\Delta G_1^0 - m_1[D]\right)}{RT}}{1 + \exp - \dfrac{\left(\Delta G_1^0 - m_1[D]\right)}{RT}} \tag{3}$$

$$A_{obs} = \frac{A_0 + A_{11}\exp - \dfrac{\left(\Delta G_1^0 - m_1[D]\right)}{RT} + A_u\exp - \dfrac{\left(\Delta G_1^0 + \Delta G_2^0 - (m_1+m_2)[D]\right)}{RT}}{1 + \exp - \dfrac{\left(\Delta G_1^0 - m_1[D]\right)}{RT} + \exp - \dfrac{\left(\Delta G_1^0 + \Delta G_2^0 - (m_1+m_2)[D]\right)}{RT}} \tag{4}$$

Here, variables ΔG^0 are the free energy changes at every step, m_i indicate the dependence of free energy on the denaturant concentration [D] and A's are the specific contributions of each species to the signals. R and T are gas constant and absolute temperature, respectively.

2.5. NMR data acquisition and processing

All NMR experiments were performed at 27 °C on a Varian *Inova* 600 MHz NMR spectrometer equipped with pulse shaping and pulse field gradient capabilities. The NMR sample was prepared in acetate buffer (20 mM, pH 3.0) containing 250 mM NaCl and 1 mM dithiothreitol (DTT). Nearly 550 μl (90% H_2O + 10% D_2O) of 1.2 mM protein was used to record NMR experiments. For the HNN [62] spectrum the delays T_N, and T_C, were both set to 28 ms. Forty complex points were used along t_1 and t_2 dimensions. The HN(C)N [62] spectrum was recorded with the same T_N and T_C parameters, same number of t_1 and t_2 points, and the T_{CC} delay was set to 9 ms. For the HNCA spectrum the delay T_N was set to 25 ms. Sixty-four and 40 complex points were used along t_2 and t_1 dimensions, respectively. The HN(CO)CA spectrum was recorded with the same T_N parameter, same number of t_2 and t_1 points, and the T_{CC} delay was set to 9 ms. TOCSY-HSQC was recorded with a mixing time of 60 ms, 32 complex points along ^{15}N (t_1) dimension and 80 complex points along ^1H (t_2) dimension. HNCO was recorded with 56 and 40 complex points along t_2 and t_1, respectively; with a T_N delay of 28 ms. An HSQC spectrum was recorded with 128 t_1 increments. NOESY-HSQC spectra were recorded with a mixing time of 150 ms, 32 complex points along ^{15}N (t_1) dimension and 80 complex points along ^1H (t_2) dimension. The relaxation experiments were carried out using the pulse sequences described by Farrow et al. [63]. In these, 2048 and 128 complex points were collected along the two dimensions. R_1 measurements were done using the following inversion recovery delays: 10, 50, 120, 220, 350, 600, 900, 1200 ms and spectra duplicated at 120 and 600 ms. For R_2 measurements, the following Carr–Purcell–Meiboom–Gill (CPMG) delays were used: 10, 30, 50, 90, 130, 150, 190, 230 ms and spectra duplicated at 50 and 150 ms. The recycle delay for R_1 and R_2 measurements was 2 s. The $R_{1,2}$ values were extracted by fitting the peak intensities to the equation, $I(t) = B\ \exp(-R_{1,2}t)$. Steady-state ^1H–^{15}N NOE experiments were carried out using an irradiation time of 3 s and a total recycle delay of 5 s for each scan. Thirty-two scans were used for each fid for signal averaging the data. The errors in the NOEs were obtained using the root mean square value of the background noise as described by Farrow et al. [63]. Data were processed using FELIX 2000 on a Silicon Graphic, Inc. work station.

2.6. NMR resonance assignments

Backbone amide and ^{15}N resonance assignments for the folded protein were obtained using the protocols based on HNN and HN(C)N [64,65]. These assignments agree with those reported earlier [53] (BioMagRes ID: BMRB-6096) and are indicated in Fig. 1. Following these amide and ^{15}N assignments, the carbon assignments were readily obtained from the well known triple resonance experiments, HNCA, HN(CO)CA, and HNCO (reviewed in Ref. [66]). The former two experiments together provide C^α assignments while the HNCO provides CO assignments. The peak assignments for the spectra in 1 M urea and 0.5 M guanidine could be readily obtained by simple transfer from the folded protein assignments. On rare occasions of ambiguities due to closeness of peaks, spin system identification by TOCSY-HSQC, helped resolve the ambiguities. In cases where the shifts were large, assignments were obtained independently from connectivities in the triple resonance spectra. Here we wish to mention that we do not have assignments for the residues Lys 9 and Glu 69 in the folded protein and for Lys 87 in 1 M urea.

2.7. Spectral density calculations and correlation times

Spectral density functions $J(0)$, $J(\omega_N)$ and $J(\omega_H)$ were calculated, as described by Lefevre et al., by reduced spectral density mapping [67]. The linear correlation between $J(0)$ and $J(\omega_N)$, and between $J(0)$ and $J(\omega_H)$ was then examined [67]. Reduced spectral density mapping uses only three ^{15}N relaxation parameters, with the assumption that at high frequencies the spectral density functions $J(\omega_H) \approx J(\omega_H + \omega_N) \approx J(\omega_H - \omega_N)$. By this approach the spectral density functions are expressed as follows:

$$J(0) = \frac{3}{2(3d' + c')}\left[-\frac{1}{2}R_1 + R_2 - \frac{3}{5}R_{NOE}\right] \tag{5}$$

$$J(\omega_N) = \frac{1}{3d' + c'}\left[R_1 - \frac{7}{5}R_{NOE}\right] \tag{6}$$

$$J(\omega_H) = \frac{1}{5d'}R_{NOE} \tag{7}$$

where,

$$R_{NOE} = (\{^1H - ^{15}N\}NOE - 1)R_1 \cdot (\gamma_N/\gamma_H)$$

The constants c' and d' are approximately equal to 1.25×10^9 (rad/s)^2 and 1.35×10^9 (rad/s)^2, respectively, at 14.1 T [68]. The errors in the spectral density functions were calculated from Eqs. (5)–(7) using the errors in the ^{15}N relaxation parameters.

An estimate of the overall correlation times characterizing the motions of the protein in the native and the near native states was obtained from the spectral density functions following a procedure described by Lefevre et al. [67]. They observed empirically that $J(\omega_N)$ and $J(\omega_H)$ show a linear correlation with $J(0)$. For example for $J(\omega_N)$ vs $J(0)$, one can write

$$J_i(\omega_N) = \alpha_N J_i(0) + \beta_N \tag{8}$$

Using this in conjunction with the basic Lorentzian definition of the spectral density function the following equation can be derived.

$$2\alpha_N\omega_N^2\tau^3 + 5\beta_N\omega_N^2\tau^2 + 2(\alpha_N - 1)\tau + 5\beta_N = 0 \tag{9}$$

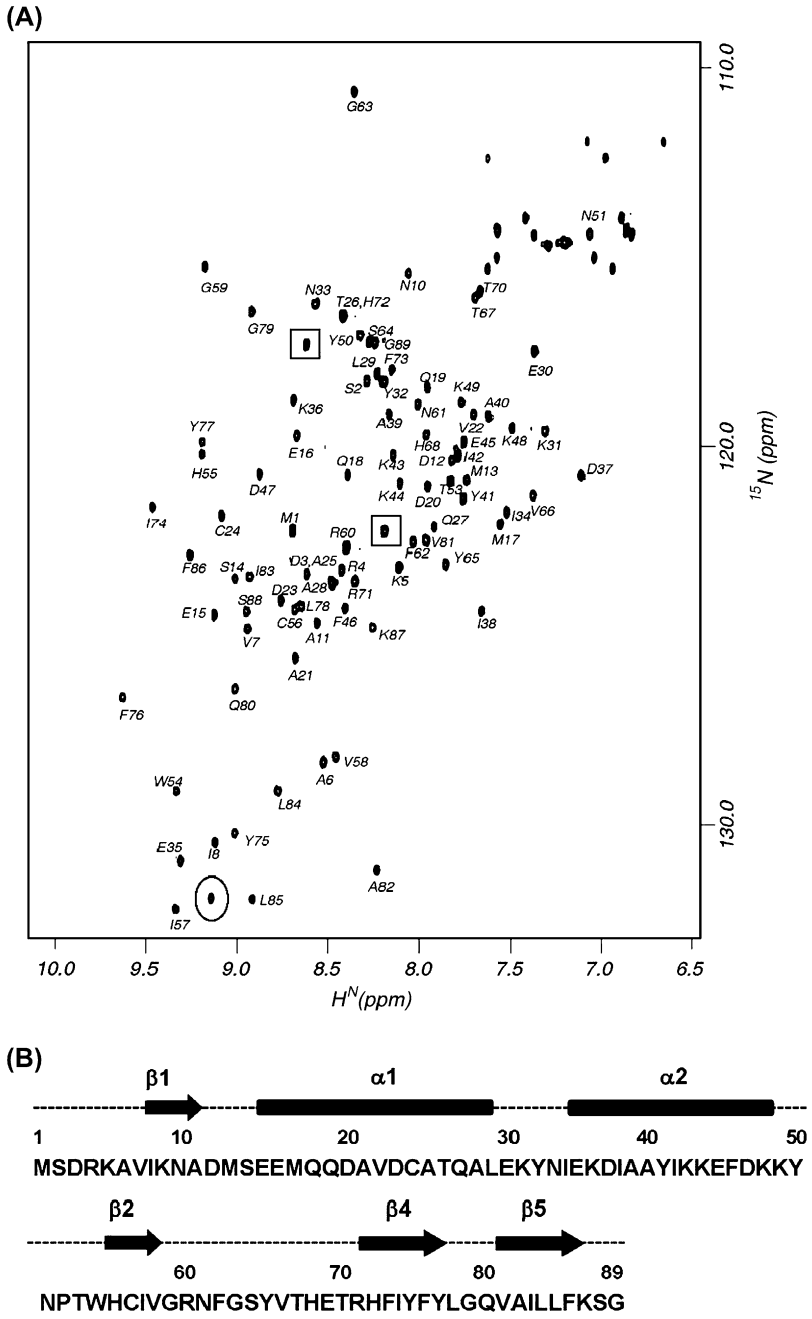

Fig. 1. (A) Finger print $^{1}H-^{15}N$ HSQC spectrum of monomeric DLC8 showing the residue specific assignments at pH 3.0, 27 °C. The peaks enclosed in squares belong to the N-terminal extension and the peak enclosed in the ellipse belongs to the W54 side chain. (B) Primary sequence of DLC8. Secondary structural elements are marked on the top of the sequence; α-helices are marked with cylinders and β-sheets are marked with arrows.

This equation can be solved to estimate the correlation time τ. A similar analysis can be performed with $J(\omega_H)$ vs $J(0)$ relation as well.

3. Results and discussion

3.1. Denaturation profile of DLC8 by circular dichroism and fluorescence

Equilibrium denaturation experiments provide an easy and convenient way of finding out whether the protein unfolding follows a simple two-state kinetics or otherwise. In the former case the profiles have typical sigmoidal shapes and have the same characteristics when monitored by different probes. Circular dichroism and steady state fluorescence have been the two most useful probes in all such studies. Often it has been observed that the denaturation profiles exhibit different baseline characteristics in the pre- and post-transition regions and this has been thought to be due to different interactions of the native (N) and the unfolded (U) states with the denaturant and their dependence on the denaturant concentrations [69]. Fig. 2 shows normalized denaturation profiles for

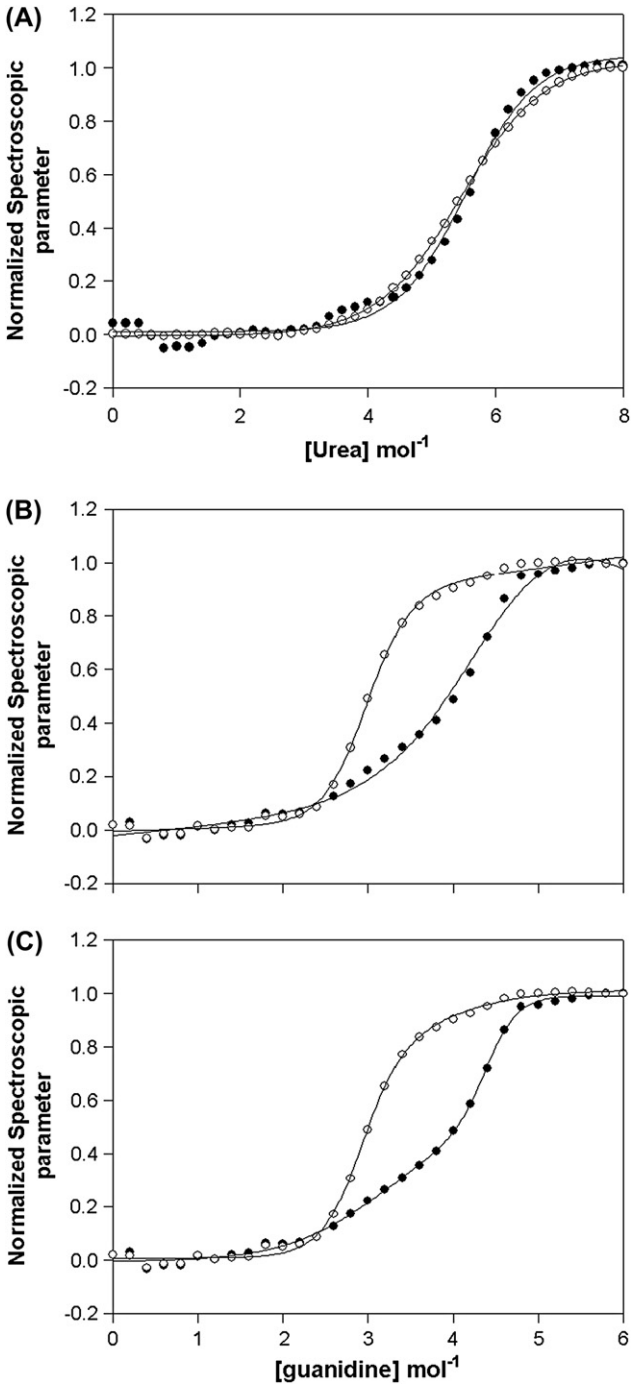

Fig. 2. Normalized spectroscopic parameters (CD and steady state fluorescence) plotted against concentration of urea (A) and guanidine hydrochloride (B, C). Filled circles represent CD data while open circles represent steady state fluorescence data. The solid lines in (A) and (B) represent fits to Eq. (3) while in (C) the lines represent fits to Eq. (4).

DLC8 (normalized using Eqs. (1) and (2) in Section 2), due to urea (A) and guanidine hydrochloride (B, C), obtained by means of far-UV CD spectroscopy (filled circles) by monitoring ellipticity at 222 nm, and by means of fluorescence spectroscopy, by monitoring tryptophan emission at 330 nm (open circles). In case of urea, as the denaturation curves obtained from both the spectroscopic parameters overlap, one can say that urea unfolding of DLC8 is a simple two-state process. On the other hand the guanidine created denaturation profiles do not overlap pointing towards a more complex unfolding by guanidine.

The urea data from both CD and fluorescence measurements (Fig. 2A) were fitted with Eq. (3) which describes a two-state unfolding process, N ↔ U. The derived thermodynamic parameters and the midpoints of the transition are summarized in Table 1. As must be expected, the transition midpoints obtained from two-state fits for CD (5.5 M) and steady state fluorescence (5.4 M) curves are similar. We also observe that in the urea induced unfolding data (Fig. 2A) there is a small hump in the CD data (∼4 M). However, this is within the range of baseline fluctuations. Moreover, our efforts to fit the CD data of urea induced unfolding to Eq. (4) resulted in high errors for the observed ΔG values (data not shown).

Considering that the CD and fluorescence denaturation curves for GdnHCl are also sigmoidal in shape, they were also fitted with Eq. (3) (Fig. 2B). Interestingly steady state fluorescence shows a transition midpoint at 3.0 M which is different from the midpoint at 4.0 M shown by CD. Thus GdnHCl unfolding is clearly more complex and must involve some intermediates. Hence we fitted the guanidine denaturation profiles to Eq. (4) as well, which describes a three-state unfolding process. The fits are shown by solid lines in Fig. 2C. The denaturation curve obtained from CD gave a good fit with a global unfolding free energy of 18 kcal mol^{-1}. However, the denaturation curve obtained by monitoring fluorescence gave a very high error for the ΔG_2 (see Table 1). Hence it appears that the fluorescence data are best described by a two-state process. This implies that the tertiary structure of the protein as sensed by fluorescence of the single tryptophan in the protein is lost in a cooperative two-state manner whereas the secondary structure is lost according to a three-state process. The first transition in the CD data corresponds roughly to the transition in the fluorescence data (∼3.0 M), indicating that along with the loss of tertiary structure there is also some loss of secondary structure. This must be expected since the single tryptophan at location 54 which is the reporter in fluorescence data is at the beginning of the β2 strand. However, as must be expected the free energy changes are not the same. Moreover the intermediates must be short-lived and hence no well-defined separate transition is seen in the CD denaturation curve. The apparent free energy difference between the folded and the unfolded states could be calculated from the above fits. These values, which are different for the two denaturants, have been summarized in Table 1. The observed difference in the free energies must be attributed to different free energies of the folded and the unfolded states in the presence of the two denaturants.

Differences of the above type in the global features of the unfolding processes by urea and guanidine have been observed previously in many proteins [44,45,47,70]. In general guanidinium hydrochloride is found to be 2–2.5 times more effective as a denaturant than urea [14,43]. A recent study by Dempsey et al. [42] on helical peptides with and without side chain electrostatic contributions to stability suggested that guanidine is

Table 1
Unfolding free energies and transition midpoints for urea and guanidine denaturation of DLC8, at pH 3.0 and 27 °C

	Guanidine hydrochloride							Urea	
	Two-state		Three-state					Two-state	
	N ⇔ U		N ⇔ I ⇔ U					N ⇔ U	
	ΔG	m	ΔG_1	m_1	ΔG_2	m_2	ΔG_{sum}	ΔG	m
CD	4.0 ± 0.3	4.0	3.3 ± 0.4	3.2	13.5 ± 1.8	4.4	16.8	6.3 ± 0.4	5.5
Fluorescence	5.8 ± 0.3	3.0	6.8 ± 1.3	3.0	4.1 ± 5.8	3.7	10.9	6.6 ± 0.4	5.4

considerably more effective than urea in destabilizing indole–indole interactions among tryptophan residues. In case of DLC8, which contains a single tryptophan residue, the tryptophan fluorescence suggested a two-state unfolding process both in urea and in guanidine, and this is possibly because once the tryptophan environment is unfolded, the fluorescence does not sense any further structural changes. However, the effectiveness of unfolding tryptophan environment by urea is less than that by guanidine as can be seen from the fact the midpoint of the transition in the former is 5.4 M, whereas that in guanidine is 3.0 M. This may have to do with a stronger interaction of guanidine than urea with the tryptophan environment. Global unfolding does not seem to be cooperative in the case of guanidine, since the CD which senses overall secondary structural changes does not follow the unfolding trace obtained by fluorescence. This suggests the presence of intermediates along the unfolding transition. Further insights into the unfolding of DLC8 and the differences in the interactions of the denaturants with the folded protein at residue level, were obtained by NMR analysis of the structural and dynamic characteristics of the native and the near native states. This is described in the following sections.

3.2. Conformational dynamics and potential unfolding initiation sites in the native state

Unfolding of a folded protein can occur on application of some external perturbations to the solution conditions, and the process would involve some expenditure of energy to cause partial destabilization of the protein structure. The unfolding would get initiated at some locations and would spread to other regions as the strength of the perturbation is increased. The most vulnerable sites for such an initiation would be those where the expenditure of energy would be the least, and intuitively the regions which are conformationally more dynamic in the folded protein would be the most likely ones.

^{15}N transverse relaxation rates (R_2) provide very direct information regarding conformational dynamics in a given protein. Conformational exchange occurring on milli- to micro-second time scale causes a prominent increase in these rates. For any given residue in the protein, the extent of this increase will depend on the magnitude of the exchange rate between the two conformations and also on the difference in the chemical shifts in hertz between the two ^{15}N sites. The increase will be maximum when the two are nearly equal and this is the so-called intermediate exchange; under such conditions the lines will get extensively broadened, sometimes beyond detection. If the chemical shift difference is much larger or much smaller than the exchange rate, then the enhancement in the R_2 value will not be very significant. In the former case, separate sharp signals would be seen for the two sites and in the latter case sharp line at the weighted average position will be seen. Thus, to first order, residues having large R_2 values compared to the average over the length of the chain would indicate potential unfolding initiation sites in the protein. We hasten to add that there could be other sites as well where the chemical shift difference between the exchanging sites is much larger than the exchange rate and these will not get detected by the R_2 criteria.

Fig. 3A shows the residue wise transverse relaxation rates in DLC8 at 27 °C. Residues Asp 3, Ala 25, Thr 26 and His 72 were not analyzed due to peak overlaps in the HSQC spectra. The data show significant variation along the sequence suggesting different motional characteristics in different regions of the protein. Though a majority of the residues have R_2 values near the average ($\sim$7.2 s^{-1}), a few residues between 10–15, 65–70 and K87 at the C-terminal have conspicuously large values; likewise Q27 has a conspicuously low R_2 value. The low R_2 value of Q27 indicates very rapid (nano-second time scale) motion of the N–H vector similar to that of the N-terminal residues; note that we do not have data for residues A25, T26 and A28 and thus Q27 appears to stand alone. Interestingly, this lies at the C-terminal end of the α1 helix and the rapid motions here would imply that this portion of the structure is relatively less stable under our experimental conditions. On the other hand the residues which show high R_2 values (N10, M13, T67, T70 and K87) would contain large contributions of conformational transitions (micro-second time scale) to their ^{15}N relaxation rates. All of these regions can be taken to indicate potential sites for unfolding initiation in the protein [71–73]. Residues N10 and K87 call for some attention due to their prominently large R_2 values compared to their immediate neighbours, which have values close to the average. The question is: how could it be that a single residue shows such a large conformational exchange without significantly perturbing the immediate neighbours? The discussion in the previous paragraph provides a rationale to this observation; this could be an example of a situation where the chemical shift difference between the exchanging sites is much larger or smaller than the exchange rate; i.e. even though the neighbouring residues are also undergoing conformational transitions, this does not show up in their transverse relaxation rates. Since we do not

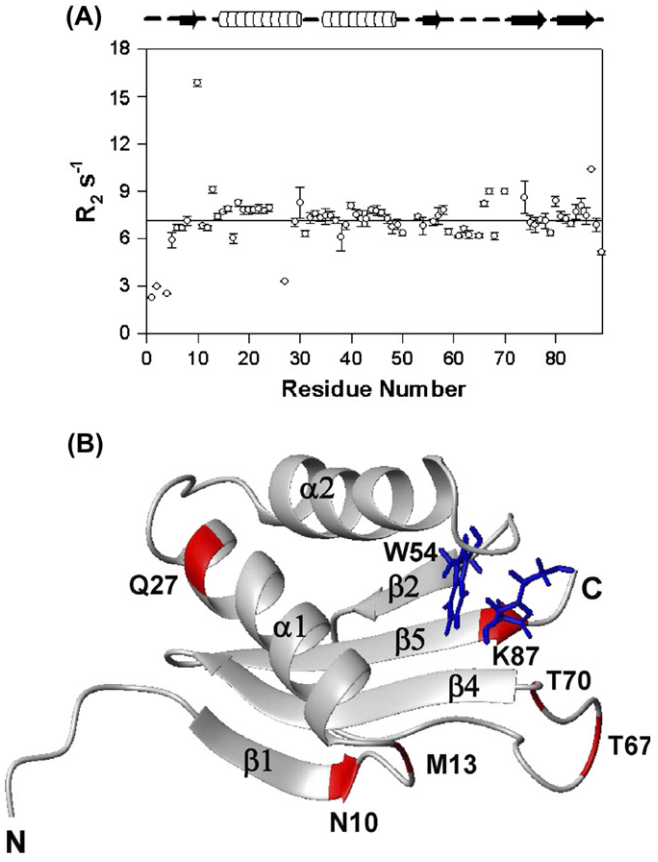

Fig. 3. (A) ^{15}N R_2 values for monomeric DLC8 at pH 3.0, 27 °C. The solid line represents the average value. (B) Native structure of monomeric DLC8 with the secondary structural elements and locations of the potential unfolding initiation sites marked. DLC8 image was produced using MOLMOL [89].

see additional peaks in the HSQC spectra, it appears that the exchange rates for the residues adjacent to N10 and K87 are much larger than the chemical shift differences between the exchanging species. Referring to the structure of the native protein (Fig. 3B), the above potential unfolding initiation sites are seen to be located in the loop between β1 and α1, at the C-terminal of α1, in the loop before β4, and in the short extended stretch at the C-terminal.

3.3. Early perturbations to the native state by urea and guanidine hydrochloride

Considering that protein unfolding would involve step wise removal of stabilizing contacts in the native protein structure, and that this could be different for the two denaturants, we investigated the residue level perturbations caused by low concentrations of the two denaturants to the native state of the protein. From far-UV CD we observed that urea unfolding transition starts at around ∼3 M, and that by guanidine starts around ∼1.5 M (see Fig. 2). We also monitored the tertiary structure unfolding from near-UV CD. These data are shown in Fig. 4. It is evident that at denaturant concentrations of up to 3 M urea and 1 M guanidine, the spectra are nearly super-imposable. However, these would not sense the small local perturbations that might occur due to specific interactions of the denaturants with the protein chain. We used a variety of NMR probes to characterize these perturbations in 1 M urea and 0.5 M guanidine both of which concentrations lie in the flat baseline regions of the denaturation curves. Henceforth, we will refer to these states created by the small denaturant concentrations as near native states.

3.3.1. Chemical shift perturbations

Chemical shifts provide the first clues to the perturbations to the protein by external agents. Fig. 5 shows overlays of the HSQC spectra of DLC8 in the native state (black contours), with that of DLC8 in 1 M urea (A) and in 0.5 M guanidine (B), both shown by red contours. Clearly, the overall patterns in the three spectra are similar but for some small shifts for a majority of the residues, indicating that the protein remains in the native state ensemble in the presence of the mentioned concentrations of the two denaturants. The appearance of extra peaks with very low intensities in Fig. 5B suggests the presence of some other minor conformers which are in slow exchange with the major species. Many of these

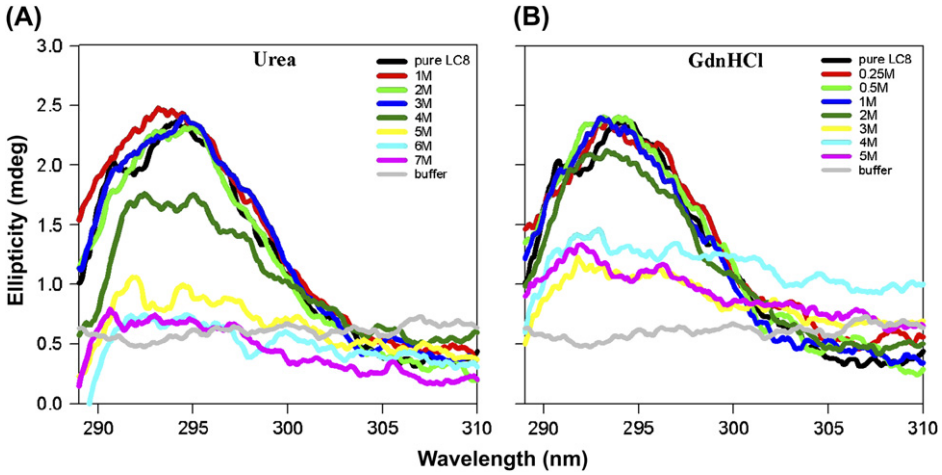

Fig. 4. Near UV-CD spectra of DLC8 at pH 3.0 at different concentrations of urea (A) and guanidine (B).

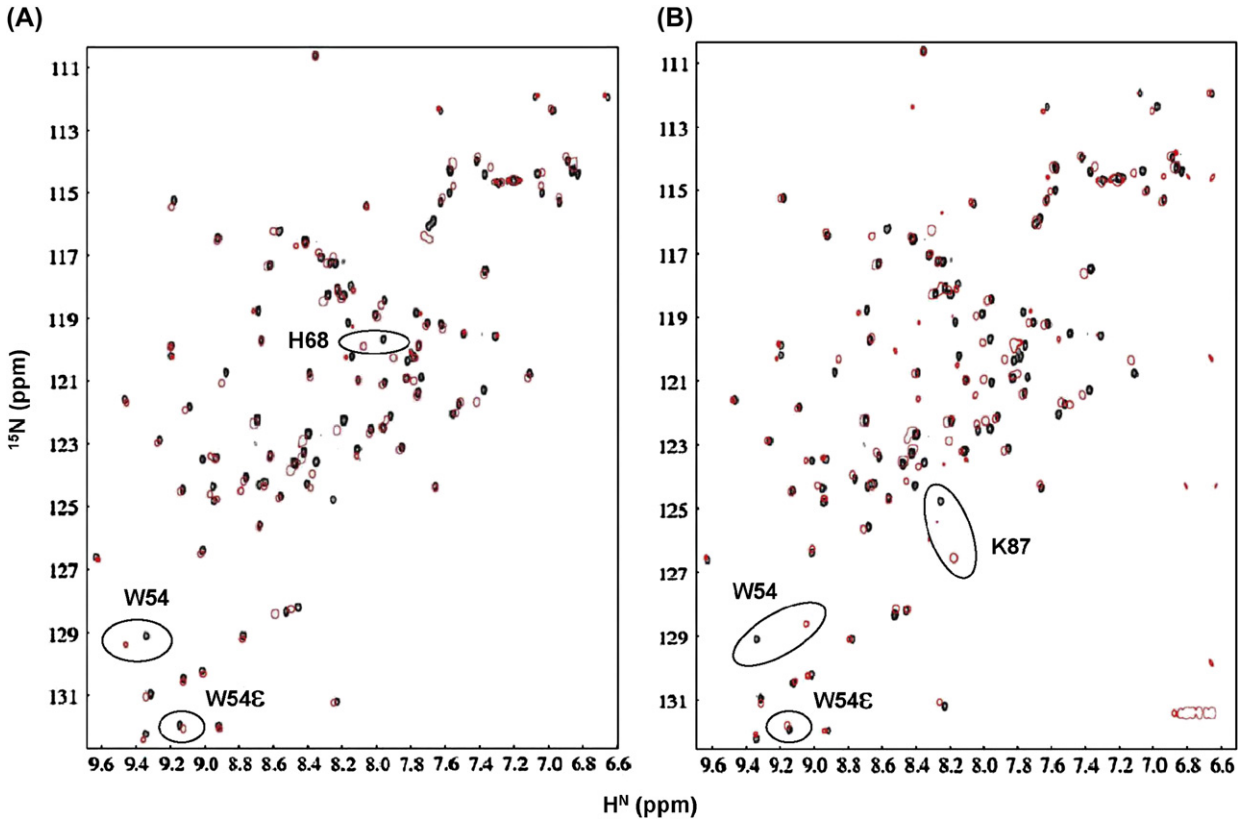

Fig. 5. Overlay of $^{1}H-^{15}N$ HSQC spectra of DLC8 at pH 3.0, 27 °C (black contours), with the spectra in the presence of the denaturants: (A) 1 M urea (red contours) and (B) 0.5 M GdnHCl (red contours). Peaks belonging to Trp 54 and His 68 in 1 M urea and Trp 54 and Lys 87 in 0.5 M guanidine which show large chemical shift changes and the side chain N–H of Trp 54 (W54ε) in both urea and guanidine have been marked with ellipses.

peaks grow in intensity when the denaturant concentration is increased to 1 M guanidine or 2 M urea, as the case may be (data not shown), along with the appearance of some additional weak peaks and also disappearance of some. This possibly suggests unfolding of the protein along multiple parallel pathways as the denaturant concentration is progressively increased. The small shifts in the peak positions of majority of the residues in the major species in the 0.5 M guanidine and 1 M urea spectra must be attributed to small local perturbations in the structural characteristics of the protein. This should include as well the local dynamics changes which would cause small changes in the average chemical shifts. Therefore, considering the changes ($\delta_F - \delta_D$) in amide ($\Delta\delta_H$) and ^{15}N ($\Delta\delta_N$) chemical shifts (δ_F and δ_D refer to chemical shifts in native and denaturing conditions, respectively), we calculated residue wise cumulative chemical shift changes ($\Delta\delta$) according to the formula:

$$\Delta\delta = \left[(\Delta\delta_H)^2 + (\Delta\delta_N/10)^2\right]^{1/2} \quad (10)$$

The factor 10 for ^{15}N chemical shift arises as a normalization factor since the overall range of nitrogen chemical shifts is roughly 10 times that of proton chemical shifts for the backbone amides in folded proteins. The results of these calculations for urea and guanidine are shown in Fig. 6A and B, respectively. The perturbed residues are also shown by color on the structure of the molecule alongside the respective panels. It appears that the deviations vary along the sequence in both the cases and this must have bearing on the different interactions of the denaturants along the polypeptide chain.

Intuitively, chemical shift perturbations at specific residues must be intimately related to exposure of the residues to the solvent, and in the present case to the denaturants. Therefore, we calculated the solvent exposed surface areas (SASA) of the individual residues following the procedure described in Ref. [74]. Considering that the surface area of a urea or a guanidine molecule is ~67 Å^2, we used a cut-off of 80 Å^2 as a conservative number to consider a particular residue as accessible to the denaturant or otherwise. The results of these are shown as solid bars in all the panels in Fig. 6. We also calculated the Kyte–Doolittle hydropathicity indices [75] for the individual residues and these are shown in Fig. 6C. It can be seen from these that all the loop areas and major portions of the α-helices are hydrophilic (negative values) and are accessible to the denaturant molecules. Therefore, one would expect all these regions to show chemical shift perturbation on addition of the denaturants. Although majority of the residues perturbed belong to the loops and the α2 helix in both the cases, there are some differences in the perturbations by the two denaturants.

Examination of the amino acid sequence of the protein reveals that it has three histidines at positions, 55, 68 and 72, and

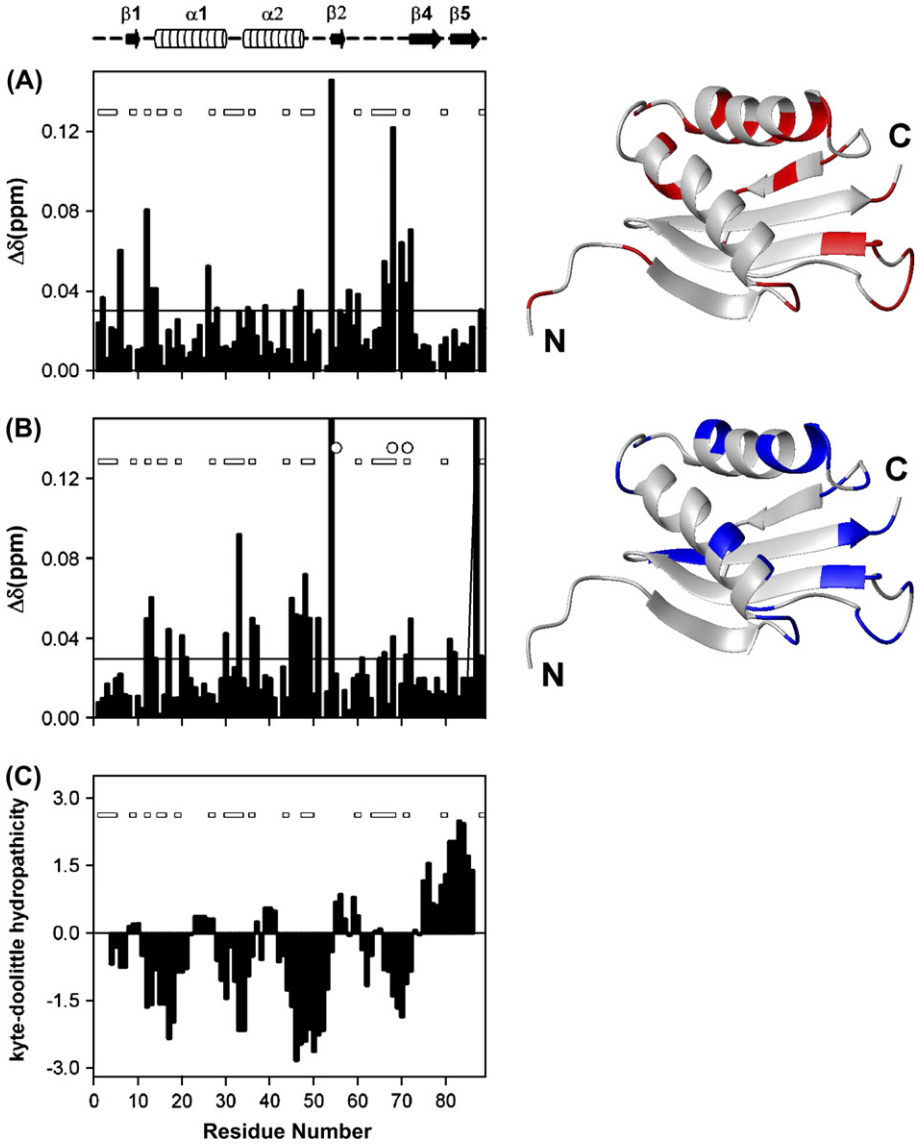

Fig. 6. Residue wise $\Delta\delta$ (see Eq. (10) in the text) for the protein in 1 M urea (A) and in 0.5 M guanidine (B), at pH 3.0, 27 °C. Changes beyond a specific cut-off (see text) have been marked by red color (1 M urea) and blue color (0.5 M guanidine) on the native structure of the protein besides the graphs. DLC8 image was produced using MOLMOL [89]. The Kyte–Doolittle hydropathicity index has been plotted in (C). Solid bars in all the panels show the SASA values >80 Å^2. Open circles in (B) show the locations of the histidine residues.

of these the last two are in the loop between β2 and β4. The pK values for the three histidines at positions 55, 68 and 72 are 4.5, 6.0 and 6.0, respectively [76], in free solution. Even though in the presence of high concentrations such as 6–8 M of denaturants, the pK values may get modified to the extent of 0.2–0.5 units [77], for the small concentrations of the denaturants as are used for the creation of near native states here these modifications would be very marginal. Thus these histidines will be protonated at pH 3 and carry a positive charge. It seems, therefore, likely that the histidines repel the incoming positively charged guanidine, and consequently, this loop region though exposed is not perturbed by the denaturant. However, we observed that the same argument could not be extended to several other residues containing charged side chains such as Arg, Lys, Asp and Glu across the polypeptide chain. One plausible reason could be that the perturbations caused by the low concentrations of the denaturants are not large enough to cause significant chemical shift changes at the backbone atoms.

It is extremely interesting that very large shift changes ($\Delta\delta$) are seen for the residues W54 ($\Delta\delta = 0.29$) and K87 ($\Delta\delta = 0.19$) (Figs. 5 and 6B); the shifted peaks in Fig. 5 were independently assigned from triple resonance spectra. These observations suggest that both guanidine and urea perturb the environments around the backbone of W54 and guanidine does that in the case of K87 as well; perhaps urea also does it but we do not know the position of K87 peak in 1 M urea spectrum. Large shifts for K87 may be anticipated considering that this site is a potential site for initial unfolding as described above and could be a preferred site of denaturant interaction. The large shifts for W54 may arise due to the fact that K87 and W54 are in close proximity on the structure of

the protein (Fig. 3B) and any perturbation at K87 would get relayed to W54. Referring to Fig. 5 we observe that the peak shifts for W54 backbone NH are in opposite directions in the two denaturants. This would imply that the specifics of the interactions, perhaps the H-bonds, are different in the two cases; guanidine is charged and has many donor hydrogens whereas urea has more hydrogen acceptor sites for the H-bonds. Thus the groups involved in the interactions could be different. While this seems logical, Fig. 5 reveals another interesting and apparently intriguing feature, namely, the peak belonging to indole side chain (circled in Fig. 5) is barely affected in both cases. In other words the environment of the indole ring of Trp side chain is not significantly affected by either of the denaturants. How could it be that the backbone of W54 is affected but not its side chain? In this context we first notice that this indole NH proton is rather unusually upfield shifted compared to its normal position around ∼10.5 ppm. That means it must be experiencing a strong shielding influence from its surroundings in the protein structure. Then, a careful examination of the protein structure revealed that this NH proton of the indole group is stacking over the aromatic ring of F46 and the aromatic ring of Y50 is also in close proximity. Further, this proton is also engaged in a strong H-bond with the backbone nitrogen of N51. Therefore, it seems likely that these stabilizing interactions are not significantly disturbed by the low concentrations used of either of the denaturants, which is why the HSQC peak of this proton is not significantly disturbed. Thus, while both urea and guanidine perturb W54 and K87, the specific interactions at those sites seem to be different. This is readily conceivable considering the different physical and chemical characteristics of urea and guanidine molecules.

Large shifts observed for H68 in the case of urea are consistent with that region also being another unfolding initiation site, but guanidine interaction at this site is possibly hindered by repulsion from charged histidine. Similarly, Y33 in guanidine and T26 in urea which are also close to another unfolding initiation site show large shift perturbations, though the urea perturbation is relatively less. The region around aa 12–14, the last of the potential unfolding sites is similarly affected by both the denaturants. Thus the structure, sequence and dynamics in the folded protein have a direct bearing on the denaturant induced unfolding process of the protein.

Next we analyzed NOESY-HSQC spectra to examine more explicitly the structural perturbations that may have occurred at those sites which exhibited significant chemical shift perturbations (colored residues in Fig. 6). We observed that in most cases, at a mixing time of 150 ms, the folded protein spectrum had the best $^{1}H-^{1}H$ NOEs and they were mostly within the residue ($H^{N}-H^{\alpha}$, H^{β}) or to nearest neighbours ($H^{N}-H^{N}$, H^{α}, H^{β}, CH_3). As an illustration we show in Fig. 7A selected strips from NOESY-HSQC spectra depicting $^{1}H-^{1}H$ NOEs from the backbone NH proton of W54, which has the maximum chemical shift perturbation in both urea and guanidine, to other protons in the protein, under the three conditions, namely, native state (i.e. in the absence of denaturants), in 0.5 M guanidine, and in 1 M urea. In Fig. 7B similar data for indole NH of W54 are shown.

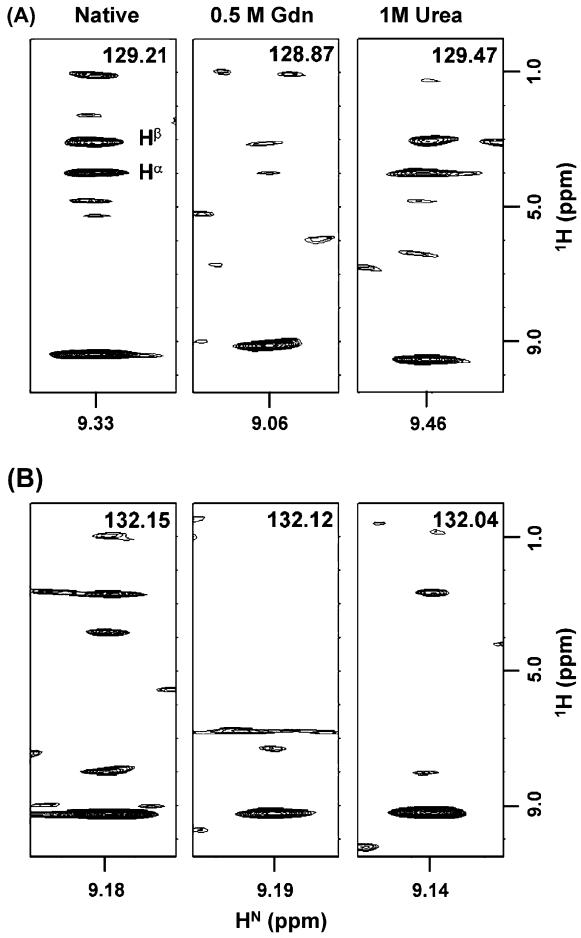

Fig. 7. Selected strips from NOESY-HSQC spectra depicting $^{1}H-^{1}H$ NOEs from backbone NH (A) and side chain indole NH (B) protons of W54 to other protons in the protein, under the three conditions, namely, native state (i.e. in the absence of denaturants), in 0.5 M guanidine, and in 1 M urea. ^{15}N chemical shifts are marked inside the strip. The numbers inside each strip indicate the ^{15}N chemical shifts at which cross sections were taken from the 3D spectra. The small differences in these numbers in (A) and (B) reflect the small shifts caused by the denaturants. Likewise there are also small shifts in the NH positions.

We see that in the strips corresponding to the native protein good NOEs are observable from the NH protons of W54 to its own H^{α} and H^{β} protons and a few weak ones to other protons. In the presence of the denaturants, however, many of these have either become weak or have disappeared. This could be either due to a reorientation of the side chain, or a consequence of the enhanced dynamics (see later) in the protein in the presence of the denaturants. This feature is observed for many other perturbed residues as well. More quantitative information on the local structural changes due to the denaturants was derived from secondary chemical shifts and torsion angle calculations as described below.

3.3.2. (ϕ, ψ) Perturbations in the near native states

We probed at residue level the structural characteristics of the near native states created by urea and guanidine hydrochloride, by using a number of NMR probes. Deviations of H^{α}, $^{13}C^{\alpha}$, and $^{13}C'$ chemical shifts of an amino acid residue in

a folded protein from their random coil values [78–81] have a well-established correlation with secondary structures. Residues which show positive (downfield) H^{α} and negative (upfield) $^{13}C^{\alpha}$ and $^{13}C'$ structure dependent chemical shift deviations (''secondary shifts'', $\Delta\delta$) map β-strands. Residues in α-helices show the opposite pattern. Actual values of chemical shifts have been used in the TALOS algorithm [82] to estimate the (ϕ, ψ) values for any given residue in a folded protein. Thus the magnitudes of the secondary shifts would also have a relation to the (ϕ, ψ) preferences in the broad secondary structural domains in the Ramachandran map. Thus to gauge the changes in these preferences on addition of the denaturants, we calculated the secondary shifts ($\Delta\delta^{s}$) for each residue as difference ($\delta_{obs} - \delta_{rc}$) between the observed chemical shift (δ_{obs}) and the corresponding sequence corrected ''random coil'' value (δ_{rc}) [78] for H^{α}, $^{13}C^{\alpha}$ and $^{13}C'$. We then calculated a cumulative secondary chemical shift, $\Delta\delta_{cum}$ as:

$$\Delta\delta_{cumm} = \Delta\delta^{s}(C^{\alpha})/20 + \Delta\delta^{s}(C')/10 - \Delta\delta^{s}(H^{\alpha})/2.5 \qquad (11)$$

where, the individual secondary shifts have been weighted by the maximum spread of the respective chemical shifts in parts per million. The residue wise comparison of the cumulative secondary shifts for the folded protein, for the protein in 1 M urea and for the protein in 0.5 M guanidine is shown in Fig. 8A–C; while we show the calculated shifts as per Eq. (9) for folded protein in A, we show the deviations from the folded protein values for the two near native states in B (urea) and C (guanidine). These reflect on the changes in the (ϕ, ψ) values. Using a cut-off of 0.3 ppm (see Section 2) for a meaningful interpretation of the cumulative secondary shifts, we observe that 1 M urea (Fig. 8B) causes fairly minor changes. About eight residues which include some in the loops between β1 and α1, and between α2 and β2 show negative deviations, whereas four residues show positive deviations. In contrast, guanidine at 0.5 M concentration (Fig. 8C) is seen to cause marked changes in the secondary shifts; about 12 and 18 residues show negative and positive deviations, respectively. The helices, around the middle portion of the protein are the most prominently perturbed. Guanidine also affects all the β-strands, though marginally, but the loop between β4 and β5 is perturbed more significantly. The various regions perturbed by the two denaturants are shown on the native structure of the protein alongside the respective panels, in a color coded manner. Many perturbations seen here coincide with those seen by chemical shift perturbations. Moreover, as seen before, there are significant differences in the effects of the two denaturants.

Then, we calculated the most probable (ϕ, ψ) values for the near native states by making use of the TALOS algorithm [82] and H^{α}, C^{α}, CO, and ^{15}N chemical shifts as inputs and we did this exercise for the folded protein as well for the purpose of comparisons. The results of TALOS predictions for the folded as well as for the two near native states are listed in the supplementary Tables SI and SII, respectively. Comparison of these results can be made using two criteria: (i) if the numbers for database fits are large and similar, then the deviations in the values larger than the width of the prediction would signify some change in the local structure, (ii) if the numbers for database fits are significantly different, then the smaller value signifies loosening of the local structure. The predicted (ϕ, ψ) values can be significantly different in this situation as well.

In the supplementary Tables SI and SII, we observe that for most cases more than six database fits were found and this provided the (ϕ, ψ) values within reasonably narrow ranges; the average widths of (ϕ, ψ) predictions for the folded state, for the 1 M urea state and for the 0.5 M guanidine state were (15.2°, 13.7°), (15.24°, 14.84°) and (18.49°, 15.43°), respectively. Using twice of these average widths as a cut-off, the ψ deviations can be used to identify changes towards β or α structures; an increase in ψ indicates a shift towards β structure while a decrease indicates a shift towards α structure. The ϕ deviations indicate structural shifts within a particular domain. These deviations in (ϕ, ψ) have been tabulated in Table 2. It can be seen that, in 1 M urea, residues N10, S14, E15, E16, K31 and F73 show noticeable shift towards α structure, while A25 shows a shift towards β structure. Likewise for the state created by 0.5 M guanidine A21, V22, D23, C24, A25, T26, E30, Y32, N33, I38, A39, A40, I42, K44, E45, R71, and H72 show shifts towards β structure, while R60, F62 and F76 show shifts towards α structure. These residues have been italicized in Table 2, which provides a quantitative measure of the structural changes. From these we conclude that the changes induced by urea and guanidine are distinctly different, both in nature and in extent, and that guanidine perturbs the helices rather significantly.

The differences in the structural perturbations listed above reflect on the extent to which local cooperativity has relayed the unfolding perturbation through the protein structure in the two cases. Continuing along these lines, it is easily deducible that the pathways of unfolding by the two denaturants would be different when the denaturant concentrations are further increased, and the global unfolding characteristics could also be correspondingly different. Indeed this is what is seen from the optical data.

3.3.3. Dynamics in the near native states

It is to be anticipated that the structural changes caused by the denaturants will be associated with some dynamic changes as well. In order to investigate such changes, we carried out ^{15}N relaxation measurements on the protein in the folded state as well as in the two near native states. Residue wise R_1, R_2, and $^{1}H-^{15}N$ steady state NOEs measured in each of the three cases are included in the supplementary Fig. S1. From this data we calculated the spectral density functions $J(0)$, $J(\omega_N)$ and $J(\omega_H)$ (see Section 2) which provide direct information on the slow (milli- to micro-second time scale), nano-second and pico-second time scale motions in the protein [67,68,83]. All these are included in the supplementary Fig. S2. For the present purpose of comparison, we show in Fig. 9A the three spectral densities in the native state, but only the deviations from the native state values, for the near native states (Fig. 9B for urea and Fig. 9C for guanidine). Interestingly, in the native state, all the spectral densities show

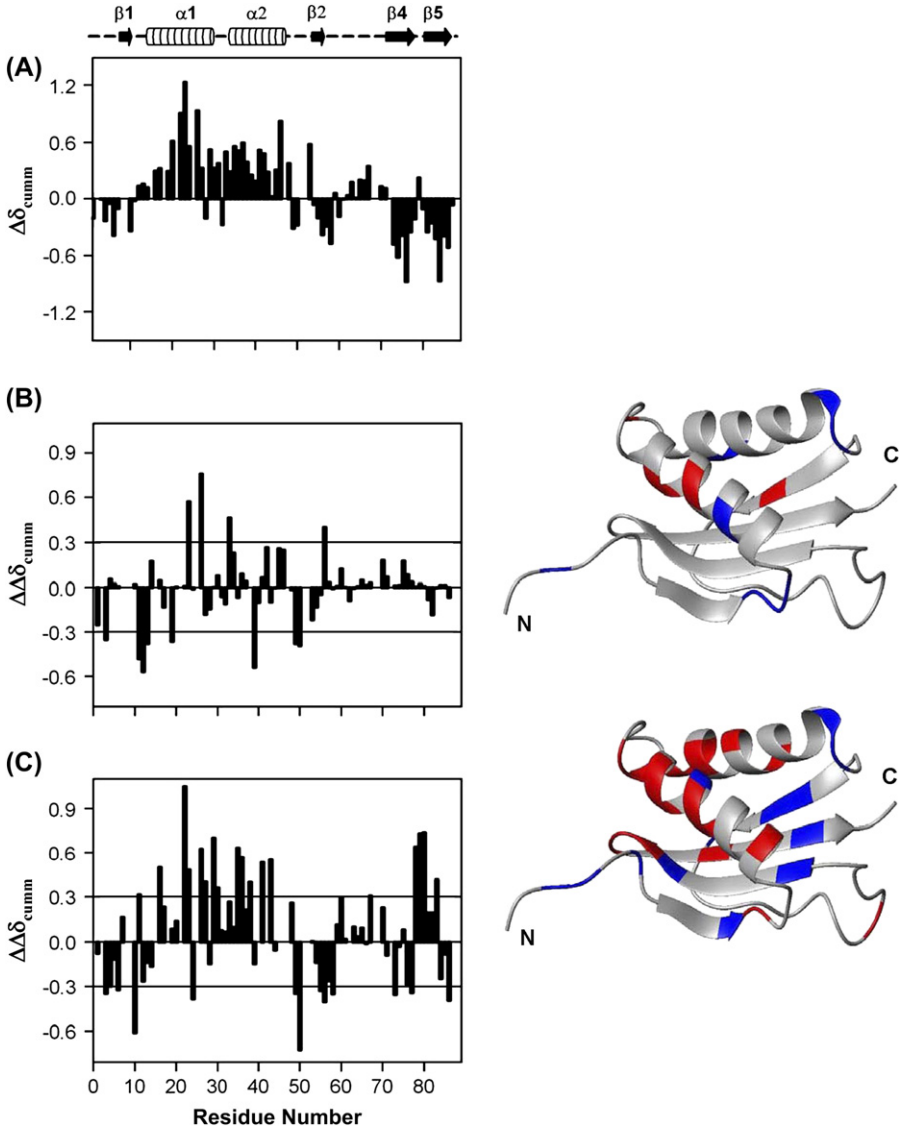

Fig. 8. (A) Cumulative secondary shifts, $\Delta\delta_{cumm}$, (see Eq. (11) in the text) for native protein. (B, C) $\Delta\delta_{cumm}$ difference from (A) for the protein in 1 M urea (B) and for the protein in 0.5 M guanidine (C), at pH 3.0, 27 °C. The native secondary structures in the protein are indicated at the top. Arrows indicate β-strands and cylinders indicate helices. Note that β3 strand does not appear here so as to maintain the same convention of strand nomenclatures in both the dimer and the monomer structures (see text). The differences are also marked on the native structure of the protein shown adjacent to the respective panels. Blue and red represent negative and positive deviations, respectively, from the secondary shifts in the native state. DLC8 image was produced using MOLMOL [89].

a fair degree of variation along the sequence, indicating significant motional variations along the chain. In the difference plots in Fig. 9B and C, negative values indicate an increase in the spectral density values in the near native state and positive values indicate a decrease. We observe that in most parts of the chain, the $J(0)$ and the $J(\omega_N)$ values increase in both the near native states, but the increase is more in the case of guanidine created state. This indicates a greater increase of flexibility and also of slow conformational transitions in the guanidine created state. The high frequency spectral density, $J(\omega_H)$, changes are even more prominently different in the two cases. While in urea there is a scatter signifying both increase and decrease, small though, in the flexibility, the guanidine perturbation seems to cause a substantial increase in the flexibility across the whole chain. These observations indicate that the denaturants cause a loosening of the protein structure even though it is still in the native state ensemble, and the loosening is more in the case of guanidine perturbation. Such global increase in residue flexibility in the presence of 0.8 M guanidine was also observed in the case of β-trefoil protein, interleukin-1β [84]. The sites which show large changes are expected to be the most vulnerable sites for further perturbation as the unfolding process continues.

An estimate of the overall correlation times characterizing the motions of the protein in the native and the near native states were obtained as described in Section 2. Fig. 10 shows the linear correlations for the three cases, namely, the native state, the 1 M urea state and the 0.5 M guanidine state of DLC8. The parameters from the regression analysis and the extracted correlation times derived from Eq. (9) are summarized in Table 3. We observe values of ∼5 ns which is a number that must be expected for the overall tumbling motion of

Table 2
TALOS predicted deviations in the ϕ (degrees) and ψ (degrees) values in the near native states from those in the folded state

Residue	ϕ (degrees)		ψ (degrees)	
	Folded − 1 M urea	Folded − 0.5 M guanidine	Folded − 1 M urea	Folded − 0.5 M guanidine
K5	0.65	0.65	−2.36	−2.36
A6	−36.67	−45.25	−1.61	5.28
V7	−6.42	−10.66	2.20	13.93
I8	−7.30	−3.52	−6.02	−15.12
K9	−4.66	−9.60	7.13	3.97
N10	−9.83	49.10	*170.92*	−0.71
A11		−1.08		−6.58
D12	11.06	−7.34	−8.82	−4.14
M13	−20.18	−36.51	25.50	0.96
S14	−44.97	−11.58	*163.38*	−6.38
E15	−36.84	−9.90	*140.87*	−14.16
E16	−38.02	−33.34	*169.49*	−6.20
M17	8.84	3.98	6.52	5.98
Q18	−0.99	0.06	1.23	−7.55
Q19	−1.14	1.45	0.14	−5.44
D20	−1.72	7.06	−1.04	−10.30
A21	−0.84	61.13	8.56	*−175.52*
V22	−16.58	38.79	29.88	*−158.73*
D23	1.41	−0.46	−1.10	*−162.27*
C24	3.14	37.75	1.06	*−208.39*
A25	1.79	10.72	*−169.65*	*−167.39*
T26	5.00	32.97	−3.91	*−173.50*
Q27	3.96	−2.57	−0.46	6.21
A28	−2.15	−4.38	1.41	4.32
L29	8.20	7.83	−14.67	−12.85
E30	−5.53	26.67	10.56	*−153.67*
K31	−24.78	−14.44	*172.88*	10.85
Y32	2.43	28.72	−6.17	*−39.09*
N33	3.25	−122.42	−0.59	*−69.32*
I34	3.08	5.95	−0.23	10.83
E35	−168.75	1.26	−22.79	−10.02
K36	−4.04	−31.15	2.95	23.61
D37	3.48	3.23	−6.51	−7.75
I38	−3.40	37.03	2.37	*−35.65*
A39	−2.89	−128.61	−1.44	*−54.52*
A40	−0.30	18.46	0.31	*−172.31*
Y41	−3.73	5.60	2.73	0.74
I42	−10.42	27.33	27.50	*−166.03*
K43	−5.43	10.45	21.25	−8.33
K44	3.91	36.57	0.76	*−44.40*
E45	−1.16	17.06	0.69	*−183.44*
F46	−1.77	3.26	−0.03	−1.44
D47	−2.75	−0.51	−7.18	1.83
K48	10.58	0.83	−11.26	2.84
K49	1.19	8.69	−4.61	−1.26
Y50	0.64	1.39	−6.50	−13.27
N51	−5.60	−1.29	6.62	1.99
P52	−31.76	−18.83	9.56	10.58
T53	17.08	−2.40	−2.97	−2.87
W54	13.36	12.02	17.44	11.49
H55	−2.87	−1.75	7.96	4.36
C56	1.49	2.19	2.76	−7.44
I57	−17.78	−11.71	−10.36	−5.17
V58	12.54	−3.65	−8.03	−9.09
G59	17.94	−29.61	−7.52	−0.07
R60	14.19	−34.23	2.85	*171.90*
N61	−0.62	−9.40	−0.08	−0.38
F62	−0.55	−31.86	1.31	*133.82*
G63	5.72	22.45	4.71	12.27
S64	−1.98	17.26	−1.34	3.65
Y65	3.21	2.20	2.01	−1.60
V66	−6.14	−5.79	12.16	−2.65
T67	4.30	−1.84	2.61	10.21
H68	3.31	1.90	1.05	−2.53
E69	−0.34	1.26	−3.58	−9.51
T70	−0.26	8.64	−6.23	−13.34
R71	−3.97	25.55	2.73	*−172.85*
H72	1.68	9.98	−18.66	*−158.09*
F73	18.33	20.53	*152.62*	−8.44
I74	−2.51	−16.48	2.96	−9.19
Y75	−1.03	−27.38	−1.92	−4.05
F76	1.63	−34.13	−3.30	*166.97*
Y77	−3.03	11.26	4.31	−4.06
L78	2.31	1.98	4.33	3.57
G79	10.77	−8.45	−4.97	6.14
Q80	0.00	−24.55	0.00	2.85
V81	0.00	26.84	0.00	−6.05
A82	−0.71	1.53	0.49	2.80
I83	−1.83	29.49	−2.36	−1.59
L84	−5.08	34.23	−1.59	−6.17
L85	−3.10	−9.28	4.04	7.45
F86	−6.65	23.07	−4.05	−4.93

a protein of this size. A smaller correlation time of ∼0.1 ns is also seen which must correspond to the interior motions in the molecule. However, there is really not much difference in the magnitudes of the correlation times between the folded and the near native states. This is consistent with the earlier inference that the protein in the presence of the denaturants at the low concentrations used still remains largely in the native state ensemble.

The above analysis presents a fairly qualitative comparison of the dynamics in the near native states which suffices, however, to show the general differences. A more quantitative comparison at residue level would warrant extension of the spectral density analysis to model-free analysis according to the formalism given by Lipari and Szabo [85,86] which would provide order parameter changes, changes in correlation times of internal motions and conformational transitions at every NH vector. This is also more appropriately done if data are recorded at more than one spectrometer frequencies. These will constitute the subject matter of future investigations.

4. Concluding remarks

Previous studies indicated that guanidine is a stronger (approximately 2–2.5 times) denaturant than urea because it destabilizes both hydrophobic and electrostatic interactions among the side chains, whereas urea possibly affects only the hydrophobic interactions [14,42]. Recent reports based largely on optical studies have investigated the mechanisms of unfolding caused by urea and guanidine in different protein and peptide model systems [42,44,47,87,88]. Effects of added salts have also been explicitly considered [42,45]. It has been

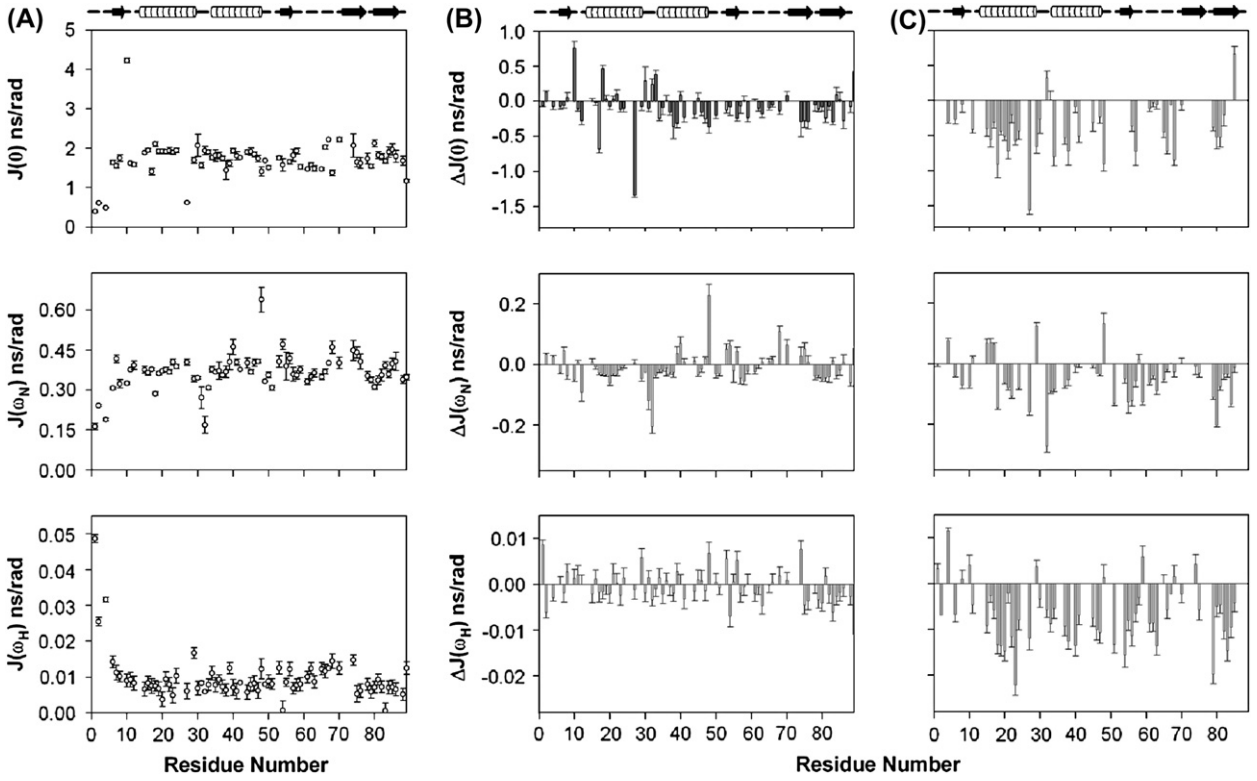

Fig. 9. Spectral density functions obtained from reduced spectral density mapping for monomeric DLC8 [67]. Calculated values of $J(0)$, $J(\omega_N)$, and $J(\omega_H)$ for the native protein are shown in (A). In (B) and (C) differences (J(native) − J(urea/guanidine)) of these values from those in 1 M urea and in 0.5 M guanidine, respectively, are plotted against residue number along the protein sequence. The native secondary structures in the protein are indicated at the top. Arrows indicate β-strands and cylinders indicate helices.

observed that depending upon the composition and the stabilizing interactions, the unfolding strength of a denaturant arises from a combination of effects on the multiple contributions to protein stability. In some, guanidine may be only slightly more effective than urea (H-bonds), and in some others such as indole−indole stacking interactions, guanidine may be far more effective [42]. Our results from optical studies on DLC8 reported here do indicate different global

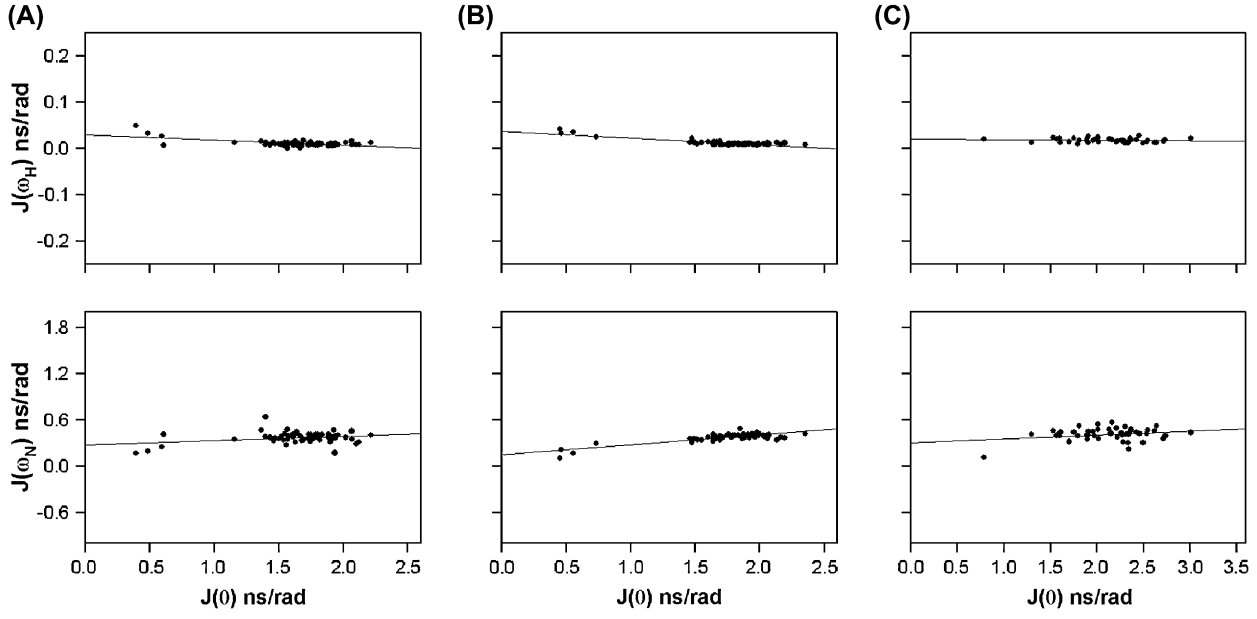

Fig. 10. $J(\omega_H)$ vs $J(0)$ and $J(\omega_N)$ vs $J(0)$ plots showing the empirical linear correlation which has been used to calculate the correlation times describing the motions in the protein. (A), (B) and (C) show these plots for folded state, 1 M urea state and 0.5 M guanidine state, respectively.

Table 3
Correlation times (τ) derived from the spectral density functions

	Folded		1 M Urea		0.5 M Guanidine	
	$J(\omega_H)$ vs $J(0)$	$J(\omega_N)$ vs $J(0)$	$J(\omega_H)$ vs $J(0)$	$J(\omega_N)$ vs $J(0)$	$J(\omega_H)$ vs $J(0)$	$J(\omega_N)$ vs $J(0)$
α	−0.011	0.055	−0.015	0.130	−0.001	0.050
β (ns/rad)	0.029	0.275	0.037	0.143	0.020	0.302
τ	0.8 ps, 1.1 ns, 5.1 ns	0.8 ns, 5.7 ns	0.1 ns, 0.8 ns, 5.2 ns	0.4 ns, 5.3 ns	0.5 ps, 1.5 ns, 33.0 ns	0.9 ns, 5.4 ns

characteristics of unfolding of the protein by the two denaturants. Our NMR characterization of the near native states created by the two denaturants provides a detailed understanding of the different interactions of the two denaturants with the protein and thus provides a rationale for the different global unfolding characteristics. The regions exhibiting slow conformational transitions serve as potential unfolding initiation sites, and different perturbations at these sites by the denaturants produce species which are slightly locally different in structure. (ϕ, ψ) changes are seen for many residues along the sequence and these are distinctly different for guanidine and urea perturbations. This also shows up in the dynamic characteristics of the two near native states. While guanidine causes a widespread increase in the flexibility across the sequence, urea causes changes in smaller pockets. These differences in turn cause different local cooperativities for further unfolding of the chain. In other words the pathways of unfolding would become different. For example, we identified that there are potential unfolding initiation sites in DLC8 near N10, Q27, H68 and K87. Specific interaction of urea and guanidine at these sites are explicitly different. Consequently further unfolding by local cooperativities in the two cases would proceed differently, and this reflects in different global unfolding characteristics by the two denaturants.

The above results, while providing an insight into the structure–dynamics interaction based mechanism for denaturant induced unfolding of DLC8, may also have implications for regulation of DLC8 function inside the cell. Since the topologies of the monomer in the functional homodimer of the polypeptide chain and of the free monomer studied here are essentially the same, different molecular signaling interactions inside the cell may stabilize or destabilize the folded structure and thus contribute to its functional regulation.

Acknowledgement

We thank the Government of India for providing financial support to the National Facility for High Field NMR at the Tata Institute of Fundamental Research.

Appendix A. Supplementary data

Supplementary data associated with this article can be found, in the online version, at doi:10.1016/j.biochi.2006.09.007.

References

[1] C.B. Anfinsen, H.A. Scheraga, Experimental and theoretical aspects of protein folding, Adv. Protein Chem. 29 (1975) 205–300.
[2] C.M. Dobson, Experimental investigation of protein folding and misfolding, Methods 34 (2004) 4–14.
[3] K. Lindorff-Larsen, P. Rogen, E. Paci, M. Vendruscolo, C.M. Dobson, Protein folding and the organization of the protein topology universe, Trends Biochem. Sci. 30 (2005) 13–19.
[4] T.K. Kumar, C. Yu, Monitoring protein folding at atomic resolution, Acc. Chem. Res. 37 (2004) 929–936.
[5] K.A. Dill, H.S. Chan, From Levinthal to pathways to funnels, Nat. Struct. Biol. 4 (1997) 10–19.
[6] C.M. Dobson, M. Karplus, The fundamentals of protein folding: bringing together theory and experiment, Curr. Opin. Struct. Biol. 9 (1999) 92–101.
[7] H.J. Dyson, P.E. Wright, Elucidation of the protein folding landscape by NMR, Methods Enzymol. 394 (2005) 299–321.
[8] D. Foguel, J.L. Silva, New insights into the mechanisms of protein misfolding and aggregation in amyloidogenic diseases derived from pressure studies, Biochemistry 43 (2004) 11361–11370.
[9] T.R. Sosnick, L. Mayne, S.W. Englander, Molecular collapse: the rate-limiting step in two-state cytochrome *c* folding, Proteins 24 (1996) 413–426.
[10] A.K. Bhuyan, J.B. Udgaonkar, Folding of horse cytochrome *c* in the reduced state, J. Mol. Biol. 312 (2001) 1135–1160.
[11] A. Chatterjee, P. Mridula, R.K. Mishra, R. Mittal, R.V. Hosur, Folding regulates autoprocessing of HIV-1 protease precursor, J. Biol. Chem. 280 (2005) 11369–11378.
[12] M. Stefani, Protein misfolding and aggregation: new examples in medicine and biology of the dark side of the protein world, Biochim. Biophys. Acta 1739 (2004) 5–25.
[13] D.J. Selkoe, Cell biology of protein misfolding: the examples of Alzheimer's and Parkinson's diseases, Nat. Cell Biol. 6 (2004) 1054–1061.
[14] C.N. Pace, Determination and analysis of urea and guanidine hydrochloride denaturation curves, Methods Enzymol. 131 (1986) 266–280.
[15] H.S. Pappa, A.E. Cass, A step towards understanding the folding mechanism of horseradish peroxidase. Tryptophan fluorescence and circular dichroism equilibrium studies, Eur. J. Biochem. 212 (1993) 227–235.
[16] S.M. Kelly, T.J. Jess, N.C. Price, How to study proteins by circular dichroism, Biochim. Biophys. Acta 1751 (2005) 119–139.
[17] C.A. Royer, Fluorescence spectroscopy, Methods Mol. Biol. 40 (1995) 65–89.
[18] C.P. van Mierlo, E. Steensma, Protein folding and stability investigated by fluorescence, circular dichroism (CD), and nuclear magnetic resonance (NMR) spectroscopy: the flavodoxin story, J. Biotechnol. 79 (2000) 281–298.
[19] C.P. van Mierlo, J.M. van den Oever, E. Steensma, Apoflavodoxin (un)folding followed at the residue level by NMR, Protein Sci. 9 (2000) 145–157.
[20] Y.O. Kamatari, R. Kitahara, H. Yamada, S. Yokoyama, K. Akasaka, High-pressure NMR spectroscopy for characterizing folding intermediates and denatured states of proteins, Methods 34 (2004) 133–143.
[21] A.R. Fersht, V. Daggett, Protein folding and unfolding at atomic resolution, Cell 108 (2002) 573–582.
[22] S.W. Englander, Protein folding intermediates and pathways studied by hydrogen exchange, Annu. Rev. Biophys. Biomol. Struct. 29 (2000) 213–238.

[23] J.K. Kamal, M. Nazeerunnisa, D.V. Behere, Thermal unfolding of soybean peroxidase. Appropriate high denaturant concentrations induce cooperativity allowing the correct measurement of thermodynamic parameters, J. Biol. Chem. 277 (2002) 40717–40721.
[24] J.K. Kamal, D.V. Behere, Thermal and conformational stability of seed coat soybean peroxidase, Biochemistry 41 (2002) 9034–9042.
[25] C.J. Mann, C.A. Royer, C.R. Matthews, Tryptophan replacements in the trp aporepressor from *Escherichia coli*: probing the equilibrium and kinetic folding models, Protein Sci. 2 (1993) 1853–1861.
[26] A. Sikorski, J. Skolnick, Dynamic Monte Carlo simulations of globular protein folding. Model studies of in vivo assembly of four helix bundles and four member beta-barrels, J. Mol. Biol. 215 (1990) 183–198.
[27] A. Sikorski, J. Skolnick, Dynamic Monte Carlo simulations of globular protein folding/unfolding pathways. II. Alpha-helical motifs, J. Mol. Biol. 212 (1990) 819–836.
[28] M. Karplus, A. Sali, Theoretical studies of protein folding and unfolding, Curr. Opin. Struct. Biol. 5 (1995) 58–73.
[29] Z. Guo, D. Thirumalai, Kinetics and thermodynamics of folding of a de novo designed four-helix bundle protein, J. Mol. Biol. 263 (1996) 323–343.
[30] J.M. Finke, J.N. Onuchic, Equilibrium and kinetic folding pathways of a TIM barrel with a funneled energy landscape, Biophys. J. 89 (2005) 488–505.
[31] A. Irback, S. Mitternacht, S. Mohanty, Dissecting the mechanical unfolding of ubiquitin, Proc. Natl. Acad. Sci. USA 102 (2005) 13427–13432.
[32] M. Roy, P.A. Jennings, Real-time NMR kinetic studies provide global and residue-specific information on the non-cooperative unfolding of the beta-trefoil protein, interleukin-1beta, J. Mol. Biol. 328 (2003) 693–703.
[33] B.A. Schulman, P.S. Kim, C.M. Dobson, C. Redfield, A residue-specific NMR view of the non-cooperative unfolding of a molten globule, Nat. Struct. Biol. 4 (1997) 630–634.
[34] C.B. Arrington, A.D. Robertson, Correlated motions in native proteins from MS analysis of NH exchange: evidence for a manifold of unfolding reactions in ovomucoid third domain, J. Mol. Biol. 300 (2000) 221–232.
[35] C.B. Arrington, A.D. Robertson, Microsecond to minute dynamics revealed by EX1-type hydrogen exchange at nearly every backbone hydrogen bond in a native protein, J. Mol. Biol. 296 (2000) 1307–1317.
[36] J. Juneja, J.B. Udgaonkar, Characterization of the unfolding of ribonuclease a by a pulsed hydrogen exchange study: evidence for competing pathways for unfolding, Biochemistry 41 (2002) 2641–2654.
[37] S. Ramachandran, B.R. Rami, J.B. Udgaonkar, Measurements of cysteine reactivity during protein unfolding suggest the presence of competing pathways, J. Mol. Biol. 297 (2000) 733–745.
[38] F.N. Zaidi, U. Nath, J.B. Udgaonkar, Multiple intermediates and transition states during protein unfolding, Nat. Struct. Biol. 4 (1997) 1016–1024.
[39] A. Chatterjee, R.V. Hosur, Following autolysis in proteases by NMR: insights into multiple unfolding pathways and mutational plasticities, Biophys. Chem. (2006).
[40] G.S. Lakshmikanth, K. Sridevi, G. Krishnamoorthy, J.B. Udgaonkar, Structure is lost incrementally during the unfolding of barstar, Nat. Struct. Biol. 8 (2001) 799–804.
[41] Y.H. Chi, T.K. Kumar, I.M. Chiu, C. Yu, Identification of rare partially unfolded states in equilibrium with the native conformation in an all beta-barrel protein, J. Biol. Chem. 277 (2002) 34941–34948.
[42] C.E. Dempsey, T.J. Piggot, P.E. Mason, Dissecting contributions to the denaturant sensitivities of proteins, Biochemistry 44 (2005) 775–781.
[43] J.K. Myers, C.N. Pace, J.M. Scholtz, Denaturant *m* values and heat capacity changes: relation to changes in accessible surface areas of protein unfolding, Protein Sci. 4 (1995) 2138–2148.
[44] N. Shukla, A.N. Bhatt, A. Aliverti, G. Zanetti, V. Bhakuni, Guanidinium chloride- and urea-induced unfolding of FprA, a mycobacterium NADPH-ferredoxin reductase: stabilization of an apo-protein by GdmCl, FEBS J. 272 (2005) 2216–2224.
[45] K. Boren, H. Grankvist, P. Hammarstrom, U. Carlsson, Reshaping the folding energy landscape by chloride salt: impact on molten-globule formation and aggregation behavior of carbonic anhydrase, FEBS Lett. 566 (2004) 95–99.
[46] J.W. Wu, Z.X. Wang, New evidence for the denaturant binding model, Protein Sci. 8 (1999) 2090–2097.
[47] M.S. Akhtar, A. Ahmad, V. Bhakuni, Guanidinium chloride- and urea-induced unfolding of the dimeric enzyme glucose oxidase, Biochemistry 41 (2002) 3819–3827.
[48] O.D. Monera, C.M. Kay, R.S. Hodges, Protein denaturation with guanidine hydrochloride or urea provides a different estimate of stability depending on the contributions of electrostatic interactions, Protein Sci. 3 (1994) 1984–1991.
[49] E.L. Holzbaur, R.B. Vallee, DYNEINS: molecular structure and cellular function, Annu. Rev. Cell Biol. 10 (1994) 339–372.
[50] E. Barbar, B. Kleinman, D. Imhoff, M. Li, T.S. Hays, M. Hare, Dimerization and folding of LC8, a highly conserved light chain of cytoplasmic dynein, Biochemistry 40 (2001) 1596–1605.
[51] P.M. Mohan, M. Barve, A. Chatterjee, R.V. Hosur, pH driven conformational dynamics and dimer-to-monomer transition in DLC8, Protein Sci. 15 (2006) 335–342.
[52] J. Liang, S.R. Jaffrey, W. Guo, S.H. Snyder, J. Clardy, Structure of the PIN/LC8 dimer with a bound peptide, Nat. Struct. Biol. 6 (1999) 735–740.
[53] M. Makokha, Y.J. Huang, G. Montelione, A.S. Edison, E. Barbar, The solution structure of the pH-induced monomer of dynein light-chain LC8 from Drosophila, Protein Sci. 13 (2004) 727–734.
[54] J.S. Fan, Q. Zhang, M. Li, H. Tochio, T. Yamazaki, M. Shimizu, M. Zhang, Protein inhibitor of neuronal nitric-oxide synthase, PIN, binds to a 17-amino acid residue fragment of the enzyme, J. Biol. Chem. 273 (1998) 33472–33481.
[55] S.R. Jaffrey, S.H. Snyder, PIN: an associated protein inhibitor of neuronal nitric oxide synthase, Science 274 (1996) 774–777.
[56] H. Puthalakath, D.C. Huang, L.A. O'Reilly, S.M. King, A. Strasser, The proapoptotic activity of the Bcl-2 family member Bim is regulated by interaction with the dynein motor complex, Mol. Cells 3 (1999) 287–296.
[57] H. Puthalakath, A. Villunger, L.A. O'Reilly, J.G. Beaumont, L. Coultas, R.E. Cheney, D.C. Huang, A. Strasser, Bmf: a proapoptotic BH3-only protein regulated by interaction with the myosin V actin motor complex, activated by anoikis, Science 293 (2001) 1829–1832.
[58] F. Schnorrer, K. Bohmann, C. Nusslein-Volhard, The molecular motor dynein is involved in targeting swallow and bicoid RNA to the anterior pole of *Drosophila oocytes*, Nat. Cell Biol. 2 (2000) 185–190.
[59] A. Ghosh-Roy, M. Kulkarni, V. Kumar, S. Shirolikar, K. Ray, Cytoplasmic dynein–dynactin complex is required for spermatid growth but not axoneme assembly in Drosophila, Mol. Biol. Cell 15 (2004) 2470–2483.
[60] R. Murugan, S. Mazumdar, Role of substrate on the conformational stability of the heme active site of cytochrome P450cam: effect of temperature and low concentrations of denaturants, J. Biol. Inorg. Chem. 9 (2004) 477–488.
[61] S. Patel, A.F. Chaffotte, F. Goubard, E. Pauthe, Urea-induced sequential unfolding of fibronectin: a fluorescence spectroscopy and circular dichroism study, Biochemistry 43 (2004) 1724–1735.
[62] S.C. Panchal, N.S. Bhavesh, R.V. Hosur, Improved 3D triple resonance experiments, HNN and HN(C)N, for HN and 15N sequential correlations in (13C, 15N) labeled proteins: application to unfolded proteins, J. Biomol. NMR 20 (2001) 135–147.
[63] N.A. Farrow, R. Muhandiram, A.U. Singer, S.M. Pascal, C.M. Kay, G. Gish, S.E. Shoelson, T. Pawson, J.D. Forman-Kay, L.E. Kay, Backbone dynamics of a free and phosphopeptide-complexed Src homology 2 domain studied by 15N NMR relaxation, Biochemistry 33 (1994) 5984–6003.
[64] N.S. Bhavesh, S.C. Panchal, R.V. Hosur, An efficient high-throughput resonance assignment procedure for structural genomics and protein folding research by NMR, Biochemistry 40 (2001) 14727–14735.
[65] A. Chatterjee, N.S. Bhavesh, S.C. Panchal, R.V. Hosur, A novel protocol based on HN(C)N for rapid resonance assignment in ((15)N, (13)C) labeled proteins: implications to structural genomics, Biochem. Biophys. Res. Commun. 293 (2002) 427–432.
[66] A.E. Ferentz, G. Wagner, NMR spectroscopy: a multifaceted approach to macromolecular structure, Q. Rev. Biophys. 33 (2000) 29–65.
[67] J.F. Lefevre, K.T. Dayie, J.W. Peng, G. Wagner, Internal mobility in the partially folded DNA binding and dimerization domains of GAL4: NMR

analysis of the N–H spectral density functions, Biochemistry 35 (1996) 2674–2686.
[68] P. Zhang, K.T. Dayie, G. Wagner, Unusual lack of internal mobility and fast overall tumbling in oxidized flavodoxin from *Anacystis nidulans*, J. Mol. Biol. 272 (1997) 443–455.
[69] D.W. Bolen, M. Yang, Effects of guanidine hydrochloride on the proton inventory of proteins: implications on interpretations of protein stability, Biochemistry 39 (2000) 15208–15216.
[70] F. Rashid, S. Sharma, B. Bano, Comparison of guanidine hydrochloride (GdnHCl) and urea denaturation on inactivation and unfolding of human placental cystatin (HPC), Protein J. 24 (2005) 283–292.
[71] N.S. Bhavesh, R. Sinha, P.M. Mohan, R.V. Hosur, NMR elucidation of early folding hierarchy in HIV-1 protease, J. Biol. Chem. 278 (2003) 19980–19985.
[72] D. Eliezer, J. Yao, H.J. Dyson, P.E. Wright, Structural and dynamic characterization of partially folded states of apomyoglobin and implications for protein folding, Nat. Struct. Biol. 5 (1998) 148–155.
[73] D. Eliezer, J. Chung, H.J. Dyson, P.E. Wright, Native and non-native secondary structure and dynamics in the pH 4 intermediate of apomyoglobin, Biochemistry 39 (2000) 2894–2901.
[74] F. Fraternali, L. Cavallo, Parameter optimized surfaces (POPS): analysis of key interactions and conformational changes in the ribosome, Nucleic Acids Res. 30 (2002) 2950–2960.
[75] J. Kyte, R.F. Doolittle, A simple method for displaying the hydropathic character of a protein, J. Mol. Biol. 157 (1982) 105–132.
[76] A. Nyarko, L. Cochrun, S. Norwood, N. Pursifull, A. Voth, E. Barbar, Ionization of His 55 at the dimer interface of dynein light-chain LC8 is coupled to dimer dissociation, Biochemistry 44 (2005) 14248–14255.
[77] D.N. Marti, Apparent pK_a shifts of titratable residues at high denaturant concentration and the impact on protein stability, Biophys. Chem. 118 (2005) 88–92.
[78] S. Schwarzinger, G.J. Kroon, T.R. Foss, J. Chung, P.E. Wright, H.J. Dyson, Sequence-dependent correction of random coil NMR chemical shifts, J. Am. Chem. Soc. 123 (2001) 2970–2978.
[79] S. Schwarzinger, G.J. Kroon, T.R. Foss, P.E. Wright, H.J. Dyson, Random coil chemical shifts in acidic 8 M urea: implementation of random coil shift data in NMRView, J. Biomol. NMR 18 (2000) 43–48.
[80] D.S. Wishart, B.D. Sykes, Chemical shifts as a tool for structure determination, Methods Enzymol. 239 (1994) 363–392.
[81] D.S. Wishart, C.G. Bigam, A. Holm, R.S. Hodges, B.D. Sykes, 1H, 13C and 15N random coil NMR chemical shifts of the common amino acids. I. Investigations of nearest-neighbor effects, J. Biomol. NMR 5 (1995) 67–81.
[82] G. Cornilescu, F. Delaglio, A. Bax, Protein backbone angle restraints from searching a database for chemical shift and sequence homology, J. Biomol. NMR 13 (1999) 289–302.
[83] J.W. Peng, G. Wagner, Mapping of the spectral densities of N–H bond motions in eglin c using heteronuclear relaxation experiments, Biochemistry 31 (1992) 8571–8586.
[84] M. Roy, L.L. Chavez, J.M. Finke, D.K. Heidary, J.N. Onuchic, P.A. Jennings, The native energy landscape for interleukin-1beta. Modulation of the population ensemble through native-state topology, J. Mol. Biol. 348 (2005) 335–347.
[85] G. Lipari, A. Szabo, Model-free approach to the interpretation of nuclear magnetic resonance relaxation in macromolecules. 2. Analysis of experimental results, J. Am. Chem. Soc. 104 (1982) 4559–4570.
[86] G. Lipari, A. Szabo, Model-free approach to the interpretation of nuclear magnetic resonance relaxation in macromolecules. 1. Theory and range of validity, J. Am. Chem. Soc. 104 (1982) 4546–4559.
[87] E.S. Cobos, V.V. Filimonov, A. Galvez, E. Valdivia, M. Maqueda, J.C. Martinez, P.L. Mateo, The denaturation of circular enterocin AS-48 by urea and guanidinium hydrochloride, Biochim. Biophys. Acta 1598 (2002) 98–107.
[88] V.K. Dubey, M.V. Jagannadham, Differences in the unfolding of procerain induced by pH, guanidine hydrochloride, urea, and temperature, Biochemistry 42 (2003) 12287–12297.
[89] R. Koradi, M. Billeter, K. Wuthrich, MOLMOL: a program for display and analysis of macromolecular structures, J. Mol. Graph. 14 (1996) 51–55.